Available online at www.sciencedirect.com
SCIENCE DIRECT®
Geochimica et Cosmochimica Acta 70 (2006) 2163–2190
Geochimica
www.elsevier.com/locate/gca

Speciation and solubility of heavy metals in contaminated soil using X-ray microfluorescence, EXAFS spectroscopy, chemical extraction, and thermodynamic modeling

Tatiana A. Kirpichtchikova [a,c], Alain Manceau [a,*], Lorenzo Spadini [a], Frédéric Panfili [a], Matthew A. Marcus [b], Thierry Jacquet [c]

[a] *Environmental Geochemistry Group, LGIT, Université J. Fourier and CNRS, BP 53, 38041 Grenoble Cedex 9, France*
[b] *Advanced Light Source, Lawrence Berkeley National Laboratory, Berkeley, CA 94720, USA*
[c] *Phytorestore—Site et Concept, Hôtel Vigée Le Brun, 8 rue du Sentier, 75002 Paris, France*

Received 16 May 2005; accepted in revised form 13 February 2006

Abstract

Synchrotron-based X-ray radiation microfluorescence (μ-SXRF) and micro-focused and powder extended X-ray absorption fine structure (EXAFS) spectroscopy measurements, combined with desorption experiments and thermodynamic calculations, were used to evaluate the solubility of metal contaminants (Zn, Cu, Pb) and determine the nature and fractional amount of Zn species in a near-neutral pH (6.5–7.0) truck-farming soil contaminated by sewage irrigation for one hundred years. Zn is the most abundant metal contaminant in the soil (1103 mg/kg), followed by Pb (535 mg/kg) and Cu (290 mg/kg). The extractability of Zn, Pb, and Cu with citrate, *S*,*S*-ethylenediaminedisuccinic acid (EDDS), and ethylenediaminetetraacetic acid (EDTA) was measured as a function of time (24 h, 72 h, 144 h), and also as a function of the number of applications of the chelant (5 applications each with 24 h of contact time). Fifty-three percent of the Zn was extracted after 144 h with citrate, 51% with EDDS and 46% with EDTA, compared to 69, 87, and 61% for Cu, and 24, 40, and 34% for Pb. Renewing the extracting solution removed more of the metals. Seventy-nine, 65, and 57% of the Zn was removed after five cycles with citrate, EDDS and EDTA, respectively, compared to 88, 100, and 72% for Cu, and 91, 65, and 47% for Pb. Application to the untreated soil of μ-SXRF, laterally resolved μ-EXAFS combined with principal component analysis, and bulk averaging powder EXAFS with linear least-squares combination fit of the data, identified five Zn species: Zn-sorbed ferrihydrite, Zn phosphate, Zn-containing trioctahedral phyllosilicate (modeled by the Zn kerolite, $Si_4(Mg_{1.65}Zn_{1.35})O_{10}(OH)_2 \cdot nH_2O$), willemite ($Zn_2SiO_4$), and gahnite ($ZnAl_2O_4$), in proportions of ~30, 28, 24, 11, and less than 10%, respectively (precision: 10% of total Zn). In contrast to Cu and Pb, the same fractional amount of Zn was extracted after 24 h contact time with the three chelants (40–43% of the initial content), suggesting that one of the three predominant Zn species was highly soluble under the extraction conditions. Comparison of EXAFS data before and after chemical treatment revealed that the Zn phosphate component was entirely and selectively dissolved in the first 24 h of contact time. Preferential dissolution of the Zn phosphate component is supported by thermodynamic calculations. Despite the long-term contamination of this soil, about 79% of Zn, 91% of Pb, and 100% of Cu can be solubilized in the laboratory on a time scale of a few days by chemical complexants. According to metal speciation results and thermodynamic calculations, the lower extraction level measured for Zn is due to the Zn phyllosilicate component, which is less soluble than Zn phosphate and Zn ferrihydrite.

1. Introduction

Soils are the major sink for metal contaminants released into the environment by anthropogenic activities. Unlike many organic contaminants, heavy metals cannot be destroyed by biogeochemical processes, and site restoration relies on their removal. Various in situ and ex situ soil cleanup technologies have been employed, of which the most common are incineration, disposal in landfill, flotation, electroremediation, bioleaching, phytoremediation, and soil washing with chemicals (Van Benschoten et al.,

* Corresponding author.
E-mail address: Alain.Manceau@ujf-grenoble.fr (A. Manceau).

0016-7037/$ - see front matter © 2006 Elsevier Inc. All rights reserved.
doi:10.1016/j.gca.2006.02.006

1997; Peters, 1999; Mulligan et al., 2001; Vandevivere et al., 2001a). Incineration and landfill, which account today for a large proportion of soil cleanup operations, may lose economic interest and public acceptance in the future because they are not environmentally acceptable when large volumes are to be treated. They are also incompatible with sustainable development precepts, since the soil resource is irremediably lost. Electroremediation and flotation are generally used to treat clayey and organic soils of low permeability (Acar and Gale, 1995; Mulligan et al., 2001). Bioleaching and phytoremediation are emerging technologies, which have low implementation costs and significant environmental benefits, but the treatment time (i.e., typically several years) is a major obstacle to gaining commercial significance (Blais et al., 1992; Cunningham and Berti, 1993; Blaylock et al., 1997; McGrath, 1998; Salt et al., 1998; Tichy et al., 1998). Soil washing is usually performed ex situ in reactors with strong mineral acids and bases, and is efficient in term of metal solubilization. However, soil fertility cannot be recovered when aggressive chemical treatments are employed because the original soil texture and biogeochemistry are destroyed irreversibly, leaving essentially an inorganic matrix that will not support revegetation (Peters, 1999).

Chelating agents having a high affinity for heavy metals, such as EDTA, CDTA, DTPA, EDDHA, EGTA, HEDTA, and NTA, are alternatives to acid–base soil washing, and can be used as a curative chemical treatment or in adjunct to another process (Peters, 1999). Chelants foster the desorption of sorbed and occluded species and the dissolution of precipitated forms until equilibrium is reached (Norvell, 1984). The amount of metal solubilized with chelating agents is at least as high as with more aggressive chemical compounds, with less undesired effects on the soil physico-chemical properties (Elliott and Brown, 1989; Cline and Reed, 1995; Ghestem and Bermond, 1998; Steele and Pichtel, 1998). Also, chelants may be used to increase the bioavailability and bioaccumulation of metals by increasing their concentration in the soil solution. Various metals and radionuclides have been targeted for chelate-enhanced phytoremediation, including Pb (Blaylock et al., 1997; Huang et al., 1997; Vassil et al., 1998; Cooper et al., 1999; Wu et al., 1999), Zn (Blaylock et al., 1997; Ebbs et al., 1997; Ebbs and Kochian, 1998; Kayser et al., 2000), Cu (Blaylock et al., 1997; Kayser et al., 2000; Thayalakumaran et al., 2003a,b,c), Cd (Blaylock et al., 1997; Ebbs et al., 1997; Kayser et al., 2000; Robinson et al., 2000), Ni, Co (Blaylock et al., 1997; Robinson et al., 1999), U (Ebbs et al., 1998; Huang et al., 1998), and Au (Anderson et al., 1998). As of today, the best results were obtained on Pb-contaminated soils using Indian mustard (*Brassica juncea* L.) in combination with EDTA (Blaylock, 2000). Soils contaminated by Cu and Zn are more difficult to treat with this technique, because these elements are more bioavailable than Pb (Lombi et al., 2001), and their presence prevents the establishment of a high-biomass crop before the application of the chelant.

Although many chelating compounds for mobilizing heavy metals have been evaluated, there remain uncertainties as to the optimal choice for full-scale application. There are many factors to consider, including extraction efficiency, potential adverse effects on living organisms, and degradability and cost of the chelating compound. In addition, one generic molecule may not exist because metal extractability by a given chelant depends on the physico-chemical properties of the soil and the molecular forms of the target metal. The molecule best suited for a certain matrix may be the worst suited for another. Time is also an issue. The short-term solubilization of metals is dominated by the most labile species, while the long-term removal is determined by the replenishment of the labile pool from more recalcitrant species. Therefore, the identification and quantification of coexisting solid metal species in the soil before and after treatment are essential to design and assess the efficiency of appropriate remediation technologies.

Metal speciation in soils has been investigated with sequential extraction procedures. In principle, this approach allows the identification and quantification of as many metal forms as there are extraction steps using chemical reagents of different binding strengths and metal-specificity. Usually, metal forms are classified into five fractions: exchangeable, carbonate, Fe-Mn oxides, organic, and residual fractions (Tessier et al., 1979). However, this approach has many pitfalls, including the dissolution of non-target phases (Ostergren et al., 1999), the incomplete dissolution of a target phase (La Force and Fendorf, 2000), the incomplete removal of dissolved species due to readsorption or reprecipitation (Ostergren et al., 1999; Calmano et al., 2001; Scheinost et al., 2002), and the possible modification of the original oxidation state of the metal or metalloid (Gruebel et al., 1988). Therefore, metal forms determined by chemical extractions are operationally defined, and they may, or may not, reflect the exact nature of the existing species. This approach also provides no information on the crystal chemical status of the metal contaminant. As useful and as often used as these 'operational speciation' methods are, there is a clear need for a robust method to reliably identify and quantify the metal species at the molecular scale in solid matrices.

Extended X-ray absorption fine structure (EXAFS) spectroscopy is well suited to investigate metal speciation in soils, sediments, and biological matter because of its element selectivity, sensitivity to the binding environment of the probed element (here Zn), detection limit as low as about 100 mg/kg for most heavy metals, no need for vacuum sample environment for elements whose atomic number is higher than about 20 (i.e., Ca), and minimal sample preparation (Cotter-Howells et al., 1994, 1999; Manceau et al., 1996, 2000a, 2002a, 2003a, 2004, 2005; O'Day et al., 1998, 2000; Foster et al., 1998; Sarret et al., 1998, 2001, 2002, 2004; Ostergren et al., 1999; Morin et al., 1999, 2001; Savage et al., 2000; Gaillard et al., 2001; Hansel et al., 2001; Ryan et al., 2001; Strawn et al.,

2002; Scheinost et al., 2002; Isaure et al., 2002, 2005; Kneebone et al., 2002; Roberts et al., 2002; Kim et al., 2003; Juillot et al., 2003; Paktunc et al., 2003, 2004; Nachtegaal et al., 2005; Panfili et al., 2005; Voegelin et al., 2005). The measured EXAFS signal is averaged over all local chemical and structural environments of the target element in the analyzed volume, which can be problematic when the metal is present in several forms (Manceau et al., 1996). Fortunately, due to the heterogeneous distribution of minerals, detrital organic matter, and living organisms in soils, the nature and proportions of metal species vary on millimeter to micron length scales, affording a means to untangle the composite EXAFS signal into single-species component spectra. Suffice it then to use an X-ray probe whose lateral dimension is commensurate with this scale of heterogeneity, as are those available at 3rd generation synchrotron facilities (Sutton et al., 1999, 2002; Manceau et al., 2002b). It is important to realize that the actual chemical and structural resolution of a microprobe is higher than its spatial resolution because sub-micrometer heterogeneities make the sample inhomogeneous at the scale of analysis. Heterogeneities at a scale larger than the resolution of the microprobe can be resolved by comparing the species obtained from the microanalyses to those detected in EXAFS spectroscopic analyses of the bulk sample. However, correct identification and quantification of all species at the macroscale relies on adequate statistical sampling at the field site.

Chemically distinct microenvironments are imaged first with synchrotron-based X-ray micro-fluorescence (μ-SXRF) to characterize elemental distributions and target points-of-interest (POIs) that differ in co-association of elements for subsequent μ-EXAFS analysis. If the incident X-ray beam has dimensions of a few tens of square micrometers, then the analyzed soil area generally contains one, and rarely more than three species, thereby increasing the probability of recording single-component EXAFS spectra (i.e., from pure species), or allowing the collection of a series of distinct multi-component spectra (i.e., from mixtures) at POIs. When more spectra than unknown species are collected, and the species proportions are sufficiently different both within and among the spectra, the number of components (species) in the system can be determined by principal component analysis (PCA). Target transformation is used to determine if a given standard spectrum is one of the components (Wasserman, 1997; Wasserman et al., 1999; Ressler et al., 2000; Manceau et al., 2002b). The proportion of each species is assessed by recording the EXAFS spectrum of several cubic millimeters from the powdered soil sample with a low spatial resolution X-ray beam (Manceau et al., 1996). Because the powder EXAFS spectrum is a weighted sum of all species spectra present in the bulk, the atomic fraction of each metal species can be obtained by linear combination fits (LCF) of this spectrum to reference spectra previously identified by PCA.

These microscopic and bulk-averaging synchrotron radiation tools have been successfully used to characterize Ni and Zn in natural (Manceau et al., 2002a, 2003a, 2004, 2005; Marcus et al., 2004) and contaminated surface and subsurface soils and sediments (Manceau et al., 2000a; Roberts et al., 2002; Isaure et al., 2002, 2005; Sarret et al., 2004; Voegelin et al., 2005; Nachtegaal et al., 2005). Here, we use this approach to determine the structural forms of Zn in the solid fraction of a soil previously used for truck farming and irrigated by sewage water for 100 years. The soil is also contaminated by Pb and Cu, and to a lesser extent by other metals and metalloids. As a result of the polymetallic and aged nature of the pollution, this soil is scientifically and technically challenging for speciation study and remediation treatment. Zn, Pb and Cu extractability were investigated first with batch extraction experiments using three chelating agents, one natural carboxylic acid, citrate, and two synthetic aminocarboxylic acids, *S*,*S*-ethylenediaminedisuccinic acid (*S*,*S*-EDDS, hereafter referred to as EDDS), and ethylenediaminetetraacetic acid (EDTA). Citrate is an easily biodegradable complexant that is exudated in the rhizosphere of many vascular plants for their nutrition (Hinsinger, 2001). EDDS is a synthetic structural *S*,*S*-isomer of EDTA which is also readily biodegradable and has been proposed as a safe and environmentally benign substitute for EDTA in soil washing (Vandevivere et al., 2001a,b; Tandy et al., 2004) and chelate-enhanced phytoremediation (Grcman et al., 2003). EDTA, the most widely studied chelating agent, was used as a reference to evaluate the efficiency of the two other chelants. The nature of dissolved and residual Zn species after the chelant treatments were determined by comparing laterally resolved (μ-EXAFS) and powder EXAFS spectra of the soil before and after chemical extraction. Results were used to formulate a phytoremediation treatment that was tested in a pilot-scale experiment, which will be reported on in a subsequent paper.

2. Materials and methods

2.1. Site description and soil samples

The studied soil comes from the Pierrelaye plain, a 1200 ha truck farming area located about 30 km northwest of Paris (France), in the heart of an urban and industrial suburb. From 1899 to 1999, this site was irrigated abundantly with untreated sewage water from the city of Paris. As a result, the entire area is now contaminated by a cocktail of heavy metals, dominated by Zn, Pb and Cu. The metal contamination is confined essentially to the ploughed layer (i.e., down to ~60 cm below the surface), and the metal content is highly variable at the hectometer, and sometimes decameter, scale. Typical concentrations of Zn range from 150 to 3,150 mg/kg, of Pb 80 to 668 mg/kg, and of Cu 50 to 390 mg/kg (Baize et al., 2002). The compositional variation is due to the variability of water flow paths relative to the geometry of the irrigation network. Within each field, the gradient of metal concentration goes downslope from irrigation outlets and generally follows the ploughing

direction, with higher metal contents mostly observed at lower elevation. A survey in 1996–1998 of the entire irrigated area revealed high heavy metal contents in vegetables, and prompted the authorities to forbid truck farming in 1999. Since then, grain corn is the only authorized crop.

An undisturbed block of about 150 cm^2 horizontal × 5 cm vertical was collected in the ploughed layer from an irrigated field. One part of the block was freeze-dried, impregnated with epoxy resin, and prepared as a 30 μm-thick micro-polished thin section for electron and X-ray microanalyses. Another part was freeze-dried, homogenized, and dry-sieved at 2 mm for chemical analyses, particle-size fractionation, and chemical treatments. The soil was separated into sand (2000–50 μm), silt (50–2 μm) and clay (<2 μm) size fractions. The sand and silt fractions were separated by wet sieving, and the clay fraction was isolated by sedimentation according to Stokes law. Chemical analyses of the bulk and size fractions were conducted on aqua regia digested samples by Inductively Coupled Plasma–Atomic Emission Spectroscopy (ICP-AES, Jobin-Yvon JY 70) for major elements and Inductively Coupled Plasma–Mass Spectroscopy (ICP-MS, Perkin Elmer 5000) for trace elements, at the Centre de Recherches Pétrographiques et Géochimiques (CNRS, Nancy, France). The bulk mineralogy was investigated by powder X-ray diffraction (XRD) using a Siemens D501 diffractometer with Co Kα radiation. Homogeneous bulk samples of the untreated soil and of the residuals after the chemical treatments described below were pressed as pellets for powder EXAFS measurements.

2.2. Chemical extraction experiments

Desorption measurements were carried out in single extraction experiments with citrate, EDDS, and EDTA according to the conditions given in Table 1. Citrate was applied as a buffer solution made from free citric acid and NaOH at pH 5.5. EDTA was used as a di-sodium salt of EDTA, and EDDS as a tri-sodium salt of EDDS. One gram (dry weight) of the <2 mm soil fraction was placed in Nalgene centrifuge tubes, in which 5 mL of 10^{-2} mol/L EDTA or EDDS, or 12.5 mL of 0.1 mol/L citrate, were poured. The initial soil pH was 6.5–7.0, and was not adjusted after adding the extractant. No attempt was made to inhibit possible microbial degradation. Since citrate, EDTA, and EDDS usually form 1:1 complexes with most heavy metals, including Zn, Cu and Pb (Francis et al., 1992; Whitburn et al., 1999; Oviedo and Rodriguez, 2003), the theoretical minimum amount of chelating agent needed to extract the three metals is equal to the sum of their molar concentrations. In practice, the chelating agent is often applied in several-fold excess to maximize metal extraction (Linn and Elliott, 1988; Wasay et al., 1998; Vandevivere et al., 2001a). EDTA and EDDS form strong complexes with heavy metals, as indicated by the high value of their metal-binding stability constants ($12.7 \leqslant \log K \leqslant 18.78$), and they also have a marked affinity for heavy metals as indicated by their high selectivity coefficient ($\log SR = 18$) relative to Ca and Fe(III), the two main competing background cations present in the soil (Table 2). Consequently, a 1.4 molar excess relative to the sum of Zn, Cu, and Pb was considered sufficient to solubilize as much as possible of these metals (Table 1). Citrate is a weaker complexant than EDDS and EDTA ($4.08 \leqslant \log K \leqslant 5.9$), and it has a lower selectivity for heavy metals, suggesting a potential interference with Ca and Fe extraction, (Table 2). For this reason, the amount of added citrate equaled 1.4 times the sum of Zn, Cu, Pb, Ca and Fe (Table 1).

Two series of metal extraction were performed. In the first, the extraction time was fixed at either 24 h, 72 h or 144 h and each extraction was performed on a separate soil sample. In the second series, five successive extractions of the same sample, each lasting 24 h, were performed by renewing the extracting solution at the start of each time interval. All extractions were carried out at room temperature, with shaking at 350 rpm, and in duplicate. The pH of the suspension was measured at the beginning and at the end of each extraction step. All supernatants were centrifuged for 15 min at 3000 rpm and filtered through 0.45 μm filters for chemical analysis by ICP-AES. The residues from centrifugation at the end of the extraction experiments were washed with 30 mL distilled-deionized water, the solids freeze-dried for EXAFS analysis, and the wash solutions discarded. The extracted metal fraction was calculated as the ratio of the amount of metal in the supernatant to the amount initially present in the soil sample.

Table 1
Chemical extraction procedures

	Extracting solution	Molar ratio chelant/sum of elements	Sample name for EXAFS
Untreated soil			×0
Citrate	0.1 M $C_6H_8O_7$ + 0.1 M NaOH (pH 5.5)[a]	1.4[d]	×Ci
EDDS	0.01 M Na_3HEDDS[b]	1.4[e]	×EDDS
EDTA	0.01 M Na_2H_2EDTA[c]	1.4[e]	×EDTA

[a] Procedure adopted from Wasay et al. (1998), and Bassi et al. (2000).
[b] Procedure adopted from Vandevivere et al. (2001a).
[c] Procedure adopted from Sun et al. (2001).
[d] Molar ratio corresponded to [chelant]/[Zn + Cu + Pb + Fe + Ca].
[e] Molar ratio corresponded to [chelant]/[Zn + Cu + Pb].

Table 2
Stability constants of metal–ligand complexes

	log *K* Ca	log *K* Fe(III)	log *K* Cu	log *K* Zn	log *K* Pb	Selectivity ratio[a] (log value)
Citrate[b]	3.50	11.50	5.90	4.98	4.08	0
EDDS[c]	4.72	22.00	18.50	13.40	12.70	18
EDTA[c]	10.81	25.10	18.78	16.50	18.00	18

[a] The selectivity ratio (SR) is defined as the ratio of the solubility of heavy metals (e.g., Zn, Cu, Pb) to that of background cations (e.g., Fe, Ca) for a given set of metal and chelant concentrations in the system (Peters, 1999). It is calculated as [ZnL + CuL + PbL]/[FeL + CaL]. A high SR value indicates a strong preference of the chelant for heavy metals.
[b] log *K* values of the equilibrium M + L = ML (where L is fully deprotonated) at 20/25 °C, for 0.1 M ionic strength from Smith and Martell (1989).
[c] log *K* values of the equilibrium M + L = ML (where L is fully deprotonated) at 20/25 °C, for 0.1 M ionic strength from Martell et al. (2001).

2.3. Electron and X-ray microanalyses (SEM-EDS and μ-SXRF)

Electron probe point microanalyses were performed on two soil thin sections at the Laboratoire de Cristallographie (CNRS, Grenoble, France) with a JEOL JSM-840 A scanning electron microscope (SEM) equipped with an energy dispersive spectrometer (EDS) allowing the detection of elements with $Z \geqslant 6$. The POIs were relocated by μ-SXRF on beamline 10.3.2 at the Advanced Light Source (ALS, Berkeley, USA), and the distribution and associations of high Z elements ($Z \geqslant 18$) in regions containing the POIs were imaged by elemental mapping at 13.1 keV. The analyzed regions were scanned with 20 μm steps and a 16 (H) × 7 (V) μm^2 (FWHM) beam size for large overview maps, and 5 μm steps and 5 (H) × 5 (V) μm^2 beam size for detailed maps. The fluorescence-yield intensity was measured using a 7-element Ge solid-state detector and normalized by the incident beam intensity (I_0) and the count time. Details of the beamline and X-ray fluorescence data treatments can be found in Manceau et al. (2002b) and Marcus et al. (2004).

2.4. Extended X-ray absorption fine structure spectroscopy (EXAFS)

The chemical forms of Zn and their proportions in the soil were determined by EXAFS spectroscopy applied at micrometer (μ-EXAFS) and macroscopic (EXAFS) scales of resolution. Fluorescence-yield Zn K-edge μ-EXAFS spectra were recorded on beamline 10.3.2 on selected POIs of the thin sections, chosen on the basis of elemental associations identified by μ-SXRF. The size of the beam was adjusted to match the sample heterogeneity at the analyzed spot. Fluorescence-yield Zn K-edge bulk EXAFS spectra of the pellet samples were recorded on the FAME beamline at the European Synchrotron Radiation Facility (ESRF, Grenoble, France) using a Canberra 30-element Ge solid-state detector and a 300 (H) × 100 (V) μm^2 (FWHM) focused beam. For all X-ray analyses, the sample was oriented to 45° from both the incident and detected X-ray beam.

2.5. EXAFS data analysis

The μ-EXAFS and powder EXAFS spectra were extracted from raw X-ray absorption spectra and normalized using standard methods (Teo, 1986). The k^3-weighted EXAFS spectra were analyzed by combining PCA with LCF of reference spectra to experimental data according to the procedure described in Manceau et al. (2002b). For this approach, an extensive database, which is a compilation of the many Zn reference compounds (both synthetic and natural) previously acquired by our team, was used (Sarret et al., 1998; Manceau et al., 2000a, 2003b, 2004, 2005; Schlegel et al., 2001a; Isaure et al., 2005; Panfili et al., 2005). This database includes primary Zn minerals (carbonate, gahnite, phalerite, willemite, zincite, zincochromite, etc.), secondary Zn minerals, Zn sorption complexes and precipitates (hydroxyapatite, hopeite, phosphate dihydrate, goethite, ferrihydrite, hematite, kerolite, montmorillonite, birnessite, etc.), and Zn organic complexes (low-molecular-weight organic acids, humic and fulvic acids, bacterial exopolymers, and fungi cell walls).

Applying PCA to the complete set of μ-EXAFS spectra collected at different POIs, it was generally possible to estimate the number of species contained in the sample without a priori knowledge of their identity. This number was estimated first using the indicator parameter, IND, which ideally reaches a minimum between primary components (i.e., combination of chemical species spectra) and secondary components (i.e., background signal) (for details, see Malinowski, 1991, and Manceau et al., 2002b). Previous studies showed that this parameter may underestimate (Manceau et al., 2002b; Panfili et al., 2005), or overestimate (Sarret et al., 2004), the real number of species. Consequently, the number of significant component species was evaluated by comparing the marginal improvement of the fit total (normalized sum-square total, Sarret et al., 2004) by successively including the next principal component to the reconstruction of the data. In addition, we verified that all selected principal components were EXAFS-like. The nature of Zn species was determined by target transformation, an operation that tests the suitability of each candidate species for inclusion in the spectral data set. The closer the transformed to the original spectrum, the most likely is the Zn species present in the sample. Finally, the nature and proportions of Zn species contained in each analyzed sample volume (i.e., POIs of the thin sections and powdered samples) were determined by LCF of the corresponding experimental EXAFS spectra to the identified Zn species EXAFS spectra. Best fits were derived by increasing incrementally the number of spectral

components, and by optimizing the fraction of each component with each increment. The best statistical solution was obtained when the fit residual parameter (R) was minimized

$$R = \frac{1}{n-m}\sum_{k=1}^{n}(k^3\chi_{\mathrm{exp}}(k) - k^3\chi_{\mathrm{model}}(k))^2, \quad (1)$$

where n is the number of data points in the fit interval, and m is the number of components (i.e., reference spectra) included in the fit. The fit interval varied between 2.5–10.5 and 2.5–11.5 $Å^{-1}$, depending on the data quality. The uncertainty in the proportion of Zn species is estimated to be approximately 10% of the total amount of Zn (Manceau et al., 2000a, 2002b; Isaure et al., 2002). Thus, species whose fractional amount is less than ~10% should be viewed with caution.

3. Results

3.1. Chemical and mineralogical characterization

The soil has a near-neutral pH (6.5–7.0) and a sandy loam texture. The 40–60 cm upper layer is black and rich in humus, and the lower layer down to 80 cm is reddish and clayey. Optical microscopic observation of the soil thin sections with natural and polarized light showed heterogeneous morphological textures with the presence of grains (quartz, calcite, feldspars), coarse organic particles, finely dispersed clay matrix, and numerous anthropogenic materials (brick residues, charcoal, industrial scoria, etc.).

Chemical and mineralogical characteristics of the soil are reported in Table 3. The bulk soil chemistry is dominated by Si ($[SiO_2] = 79.6\%$), followed by Ca ($[CaO] = 3.4\%$), and Al ($[Al_2O_3] = 2.5\%$). Iron comes in fourth position with a concentration ($[Fe_2O_3] = 2.0\%$) lower than the average concentration reported for French soils (3.6%) (Baize, 2000). The soil has unusually high organic carbon content ($[C_{org}] = 3.3\%$), in comparison to most sandy ploughed soils (0.7–1.0%) (Baize, 2000). Phosphorus content is also uncommonly elevated ($[P_2O_5] = 0.6\%$), in comparison to its average value in soils (0.05%) (Sutton et al., 1999). The higher amounts of C_{org} and P probably result from long-term fertilization and intensive crop production. The most abundant trace elements are Zn (1103 mg/kg), Pb (535 mg/kg), and Cu (290 mg/kg). These values are on the higher side of the concentration range measured in the whole irrigated area, and intermediate between those reported for nearby agricultural soils (34–63 mg/kg Zn, 18–43 mg/kg Pb, and 8–19 mg/kg (Cu) (Baize et al., 2002), and soils impacted by smelting activities (2746–21,078 mg/kg for Zn, 406 mg/kg for Cu, and 8876–9135 mg/kg for Pb) (Thiry and Van Oort, 1999; Manceau et al., 2000a; Roberts et al., 2002; Juillot et al., 2003; Sarret et al., 2004). Consequently, the contamination of the studied soil can be regarded as moderate and diffuse.

The mineralogy of the bulk soil is dominated by quartz and calcite, mixed with minor amounts of albite, microcline, and phyllosilicate. No metal bearing phases were observed by XRD. The particle size distribution consists of 69% sand, 23% silt, and 8% clay in weight. Calculation of elemental distribution among soil size fractions shows that the silt and clay fractions are the main reservoirs of heavy metals. The silt fraction contains 41% of total Zn, 47% of total Cu, and 43% of total Pb. Although the clay fraction represents only 8% of the soil weight, it contains 42% Zn, 35% Cu, and 42% Pb.

3.2. Metal extractability

After 24 h of reaction time, the extractability of metals ranks in the order Cu > Zn > Pb for the three chelating agents (Fig. 1). The higher extraction of Cu is consistent with the higher stability of Cu–ligand complexes for the three chelants, as indicated by $\log K$ values (Table 2). However, the relative stability of the three Cu–ligand complexes cannot explain the differences observed among chelants. For example, EDDS, whose complex with Cu is almost as strong as that with EDTA, extracted more Cu (73%) than EDTA (51%). Also, citrate extracted almost the same amount of Cu as EDTA (55 vs. 51%), although the two Cu complexes have a 13 order of magnitude difference in binding strength (Table 2). Similar discrepancies between stability constant values and metal extractability are observed for Zn. Despite the marked contrast in $\log K$ (Zn) values,

Table 3
Chemical and mineralogical characteristics of the soil

Particle size distribution (wt.%)		Element concentrations in the <2 mm soil fraction								
		(mg/kg)			(%)					
		Zn	Cu	Pb	SiO_2	CaO	Al_2O_3	K_2O	Fe_2O_3	P_2O_5
		1103	290	535	79.6	3.4	2.5	0.6	2.0	0.6
		Element distributions into soil size fractions[a] (wt.%)								
Sand (2000–50 μm)	69	17	18	15	79	23	27	34	25	20
Silt (50–2 μm)	23	41	47	43	18	55	44	49	39	41
Clay (<2 μm)	8	42	35	42	3	22	29	17	36	39

[a] Mass distribution of elements in the soil size fractions calculated as $C_f \times M_f/C_{tot}$, where C_f is the element concentration in the fraction, M_f is the mass percentage of the fraction, and C_{tot} is the element concentration in the bulk soil.

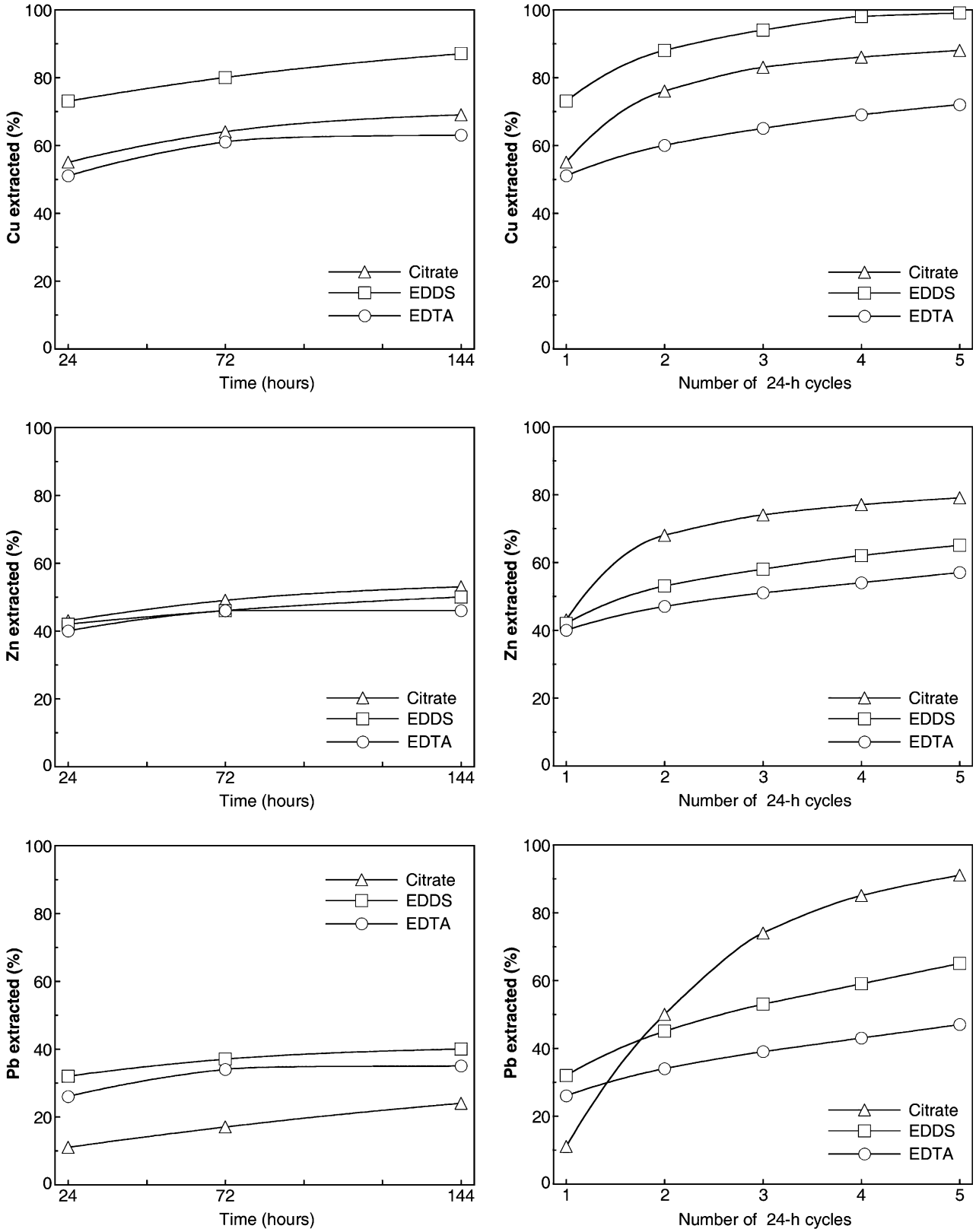

Fig. 1. Percentage of Zn, Cu and Pb solubilized by chemical extractions as a function of extraction time (left) and number of 24 h sequential extraction cycles (right). The deviations within duplicates are too small to be plotted as error bars (<1%).

which range over a factor of three, the three chelating agents extracted a similar proportion of Zn: 43% (citrate), 42% (EDDS), and 40% (EDTA) after 24 h. Likewise, the low extractability of Pb (32% with EDDS, 26% with EDTA, and 11% with citrate), compared to Cu and Zn, cannot be explained by $\log K$ (Pb) values because these

are similar in value to those of Zn and Cu. This suggests that part of the Pb pool is more tightly bound to soil constituents than the other metals, possibly as pyromorphite or some other Pb-phosphate phases, given the low solubility of lead-containing phosphates, their reported occurrence in lead-impacted soils, and the exceptionally high amount of P in the soil (Cotter-Howells et al., 1994; Hettiarachchi et al., 2000; Buatier et al., 2001; Ryan et al., 2001). More generally, two reasons may be invoked for the lack of correlation between metal extractability and the affinity of the organic ligand for the metal as measured in pure solution: one is competitive binding of other cations (e.g., Fe, Ca) to the chelant, and the second is that heavy metals are bound unevenly to several constituents having different solubilities. These hypotheses were tested using equilibrium solubility calculations and are presented in Section 4.

Increasing the extraction time over 24 h increased the extracted amounts with a moderate dependence on the chelant and metal (Fig. 1). Metal extraction increased by 9% of the initial amount of metal for Cu, 6% for Zn, and 8% for Pb after 72 h of reaction time with EDTA, and leveled off after 144 h. With EDDS, the extraction increased by 7% for Cu, 3% for Zn, and 5% for Pb after 72 h, and then again by 7% for Cu, 6% for Zn, and 3% for Pb after 144 h. With citrate, the extraction of Cu, Zn, and Pb increased by 9, 6, and 6%, respectively, after 72 h, and again by 5, 4, and 7% after 144 h (the variation between the two replicates is <1%). Finally, the proportions of Cu, Zn, and Pb extracted after 144 h equaled 69, 53, and 24% with citrate, 87, 51, and 40% with EDDS, and 61, 46, and 34% with EDTA, respectively. In summary, increasing the reaction time from 24 to 144 h increased the extraction yields by only minor amounts.

Renewing the extracting solution greatly increased the dissolved metals, but not by the same amount for the three chelants: the solubilization curves had a logarithmic shape with citrate, and were almost linear with EDDS (with the exception of Cu) and EDTA (Fig. 1, Table 4). The proportions of Cu, Zn, and Pb removed from the soil after the five extraction cycles were, respectively, 88, 79, and 91% with citrate, 100, 65, and 65% with EDDS, and 72, 57, and 47% with EDTA. Renewing the citrate solution had a tremendous effect on Pb extraction since only 11% of Pb was extracted after the first cycle, while the second and third cycles solubilized 39 and 24% from the remaining amount of Pb after the first cycle, leading to a cumulative extraction of 91% after five cycles. The successive extraction of Zn and Cu from one cycle to another was lower than that of Pb, since the first cycle with citrate extracted 43% Zn and 55% Cu, the second 25% Zn and 21% Cu from the left over, the third 6% Zn and 7% Cu, and the last even less, as indicated by the logarithmic shape of the curves. These data, together with the fact that citrate, in combination with bicarbonate (i.e., citrate–bicarbonate reagent), is known to promote the dissolution of poorly crystalline Fe oxyhydroxides (Soulier et al., 1994; Trolard et al., 1995), all collectively suggest that Pb is also associated with disordered Fe oxyhydroxides, in addition to phosphates. This interpretation is consistent with the Cu-like and Zn-like shape of the Pb extraction curves with EDDS and EDTA since these two organic ligands do not selectively dissolve poorly crystalline Fe oxyhydroxides. Equilibrium calculations presented in Section 4.2 support this interpretation.

In summary, desorption experiments showed that at least 11% and at most 100% of the metals could be removed from the soil with chelating agents, and that the extraction efficiency was higher when the chelating solution was renewed. Renewing the solution limits re-adsorption of the desorbed moieties, and increases the dissolution rate of any metal-containing particles by maintaining undersaturated conditions as in stirred-flow extractions (Strawn and Sparks, 2000). These two protocols cause desorption of metals that are held more strongly by soil constituents than surface complexes. The nature of the Zn-containing solid phases before and after extraction are identified below by μ-SXRF and EXAFS spectroscopy.

3.3. Metal partitioning and chemical associations

Bicolor (RB, Red–Blue) and tricolor (RGB, Red–Green–Blue) μ-SXRF maps of the lateral distribution of Zn and Pb (R), Cu (B), and Fe (G) in two representative regions of the soil thin sections are presented in Fig. 2. The soil texture is heterogeneous as shown by the presence of several millimeters to submillimeter elongated and rounded features, dispersed in a silty to clayey matrix. These features have a different chemical composition in RB representation, some are concentrated in Cu (i.e., blue) and others in Zn or Pb (i.e., red). The elongated blue feature in the first region (Fig. 2a) was identified by optical microscopy and SEM-EDS as root debris. Point X-ray fluorescence analysis indicated a Cu(Kα):Zn(Kβ):Pb(Lα) ratio of 100:20:22 in this area. Its color remained blue when Fe was added in green in a tricolor (RGB) representation, indicating a low Fe concentration, in contrast to the matrix. The association of Cu with root debris suggests the existence of a Cu complex with organic matter. Many occurrences of Cu-containing root debris and detrital organic structures were observed in the two thin sections.

The reddish to purple (mix of red and blue) cast of the maps in RB representation shows that, with one exception (grain POI #17), Zn and Pb are evenly distributed throughout the soil matrix. The occurrence of yellow and orange (mix of red and green) spots (i.e., POIs #5, #9, #11, #13) in RGB representation indicates that Zn and Pb are associated partly with Fe, but in amounts that vary greatly from one point to another. Some spots are green, suggesting that they are aggregates of Fe oxyhydroxides. In addition, Fe is present everywhere in the clayey matrix along with Zn, Pb, and Cu, as indicated by the brownish shade of the two tricolor maps. The almost uniform color of the matrix reveals that the soil is permeated with Fe, as is commonly observed (Singh and Gilkes, 1996; Manceau et al., 2004, 2005), but also with heavy metals. This elemental distribution suggests a structural or physical association

Table 4
Aqueous concentrations (mol/L) in supernatants for cycling extraction experiments

	EDTA exposure, cycle number				
	1 (24 h)	2 (24 h)	3 (24 h)	4 (24 h)	5 (24 h)
$[Ca]_{aq}$	4.67×10^{-3}	5.79×10^{-3}	6.31×10^{-3}	6.41×10^{-3}	5.71×10^{-3}
$[Fe]_{aq}$	2.48×10^{-4}	2.31×10^{-4}	2.35×10^{-4}	2.35×10^{-4}	2.93×10^{-4}
$[Al]_{aq}$	2.10×10^{-5}	2.51×10^{-5}	2.85×10^{-5}	3.26×10^{-5}	3.90×10^{-5}
$[Mg]_{aq}$	2.30×10^{-4}	1.85×10^{-4}	1.61×10^{-4}	1.53×10^{-4}	1.45×10^{-4}
$[Ti]_{aq}$	1.46×10^{-6}	1.59×10^{-6}	1.54×10^{-6}	1.53×10^{-6}	1.35×10^{-6}
$[Zn]_{aq}$	1.36×10^{-3}	2.27×10^{-4}	1.35×10^{-4}	9.99×10^{-5}	1.07×10^{-4}
$[Cu]_{aq}$	4.64×10^{-4}	8.74×10^{-5}	4.51×10^{-5}	3.34×10^{-5}	3.07×10^{-5}
$[Pb]_{aq}$	1.33×10^{-4}	4.27×10^{-5}	2.68×10^{-5}	2.06×10^{-5}	2.18×10^{-5}
$[P]_{aq}$	9.37×10^{-4}	1.69×10^{-4}	9.88×10^{-5}	8.97×10^{-5}	8.97×10^{-5}
Σ[MVC]	7.12×10^{-3}	6.58×10^{-3}	6.94×10^{-3}	6.99×10^{-3}	6.34×10^{-3}
$[Ca]_{aq}/\Sigma$[MVC], %	66	88	91	92	90
$[Ca]_{aq}/([Ca]_{aq} + [Fe]_{aq})$, %	95.0	96.2	96.4	96.5	95.1
	EDDS exposure, cycle number				
	1 (24 h)	2 (24 h)	3 (24 h)	4 (24 h)	5 (24 h)
$[Ca]_{aq}$	2.54×10^{-3}	2.93×10^{-3}	2.84×10^{-3}	2.65×10^{-3}	2.53×10^{-3}
$[Fe]_{aq}$	1.80×10^{-3}	1.23×10^{-3}	1.03×10^{-3}	1.04×10^{-3}	1.03×10^{-3}
$[Al]_{aq}$	1.25×10^{-3}	8.70×10^{-4}	5.85×10^{-4}	5.25×10^{-4}	3.18×10^{-4}
$[Mg]_{aq}$	7.70×10^{-4}	2.84×10^{-4}	1.23×10^{-4}	8.52×10^{-5}	4.46×10^{-5}
$[Ti]_{aq}$	5.34×10^{-6}	6.10×10^{-6}	5.07×10^{-6}	5.34×10^{-6}	4.05×10^{-6}
$[Zn]_{aq}$	1.43×10^{-3}	3.50×10^{-4}	1.64×10^{-4}	1.35×10^{-4}	1.19×10^{-4}
$[Cu]_{aq}$	6.68×10^{-4}	1.40×10^{-4}	5.18×10^{-5}	3.67×10^{-5}	2.89×10^{-5}
$[Pb]_{aq}$	1.67×10^{-4}	6.56×10^{-5}	3.96×10^{-5}	3.35×10^{-5}	3.23×10^{-5}
$[P]_{aq}$	1.35×10^{-3}	7.70×10^{-4}	7.94×10^{-4}	8.11×10^{-4}	8.49×10^{-4}
Σ[MVC]	8.63×10^{-3}	5.87×10^{-3}	4.84×10^{-3}	4.51×10^{-3}	4.10×10^{-3}
$[Ca]_{aq}/\Sigma$[MVC], %	29	50	59	59	62
$[Ca]_{aq}/([Ca]_{aq} + [Fe]_{aq})$, %	58.5	70.4	73.5	71.9	71.1
	Citrate exposure, cycle number				
	1 (24 h)	2 (24 h)	3 (24 h)	4 (24 h)	5 (24 h)
$[Ca]_{aq}$	1.37×10^{-2}	4.83×10^{-3}	1.94×10^{-3}	6.42×10^{-4}	3.17×10^{-4}
$[Fe]_{aq}$	2.27×10^{-3}	2.57×10^{-3}	9.87×10^{-4}	4.61×10^{-4}	2.87×10^{-4}
$[Al]_{aq}$	8.46×10^{-4}	5.90×10^{-4}	2.89×10^{-4}	1.56×10^{-4}	1.61×10^{-4}
$[Mg]_{aq}$	5.11×10^{-4}	5.89×10^{-4}	7.58×10^{-4}	3.74×10^{-4}	2.06×10^{-4}
$[Ti]_{aq}$	5.21×10^{-6}	1.13×10^{-5}	6.41×10^{-6}	2.57×10^{-6}	2.47×10^{-6}
$[Zn]_{aq}$	5.87×10^{-4}	3.30×10^{-4}	8.92×10^{-5}	3.37×10^{-5}	2.07×10^{-5}
$[Cu]_{aq}$	2.02×10^{-4}	7.58×10^{-5}	2.55×10^{-5}	1.13×10^{-5}	6.92×10^{-6}
$[Pb]_{aq}$	2.36×10^{-5}	8.04×10^{-5}	4.84×10^{-5}	2.32×10^{-5}	1.32×10^{-5}
$[P]_{aq}$	1.55×10^{-3}	1.57×10^{-3}	5.75×10^{-4}	1.72×10^{-4}	4.43×10^{-5}
Σ[MVC]	1.82×10^{-2}	9.08×10^{-3}	4.15×10^{-3}	1.70×10^{-3}	1.01×10^{-3}
$[Ca]_{aq}/\Sigma$[MVC], %	76	53	47	38	31
$[Ca]_{aq}/([Ca]_{aq} + [Fe]_{aq})$, %	85.8	65.3	66.3	58.2	52.5

of Zn, Pb and Cu with ferruginous clay particles. The typical Zn(Kα):Cu(Kα):Pb(Lα):Fe(Kα) ratio is 30:10:12:100.

The Zn–Fe and Pb–Fe associations imaged by μ-SXRF were confirmed by the calculation of cross-correlation values (ρ), which were high in the first mapped region ($\rho_{Zn-Fe} = 0.78$, $\rho_{Pb-Fe} = 0.71$, $\rho_{Zn-Pb} = 0.80$) and moderate in the second region ($\rho_{Zn-Fe} = 0.53$, $\rho_{Pb-Fe} = 0.57$, $\rho_{Zn-Pb} = 0.64$). The lower ρ values in the second region suggest that some Zn and Pb is not correlated with Fe. The EDS spectra collected at POIs #5, #9 and #17 show highly contrasting Zn(Kα):Fe(Kα) ratios: 55:100 at POI #5, 16:100 at POI #9, and 100:45 at POI #17 (Figs. 3a–c). If a Zn-containing Fe oxyhydroxide species exists, then it is most likely mixed with other species in variable proportions from point to point. The EDS spectrum collected at the large coffee bean feature (#17) about 300 μm in diameter exhibited an intense Zn fluorescence peak, and low intensity Cu and Pb peaks (Zn(Kα):Cu(Kα):Pb(Lα) equal to 100:23:6) (Fig. 3d). This feature is also depleted in Fe relative to the matrix ($Fe(K\alpha)_{area}$:$Fe(K\alpha)_{matrix} = 50:100$), suggesting that Zn is probably not associated with the Fe. This result partly explains the lower ρ_{Zn-Fe} value of the second region. Since light elements are not easily detected on the 10.3.2 hard X-ray microprobe, SEM was used to complete the analysis of the coffee bean. An intense X-ray line with a Zn(Kα):P(Kα) ratio of 17:100 suggests a Zn phosphate (Fig. 3d). This grain also

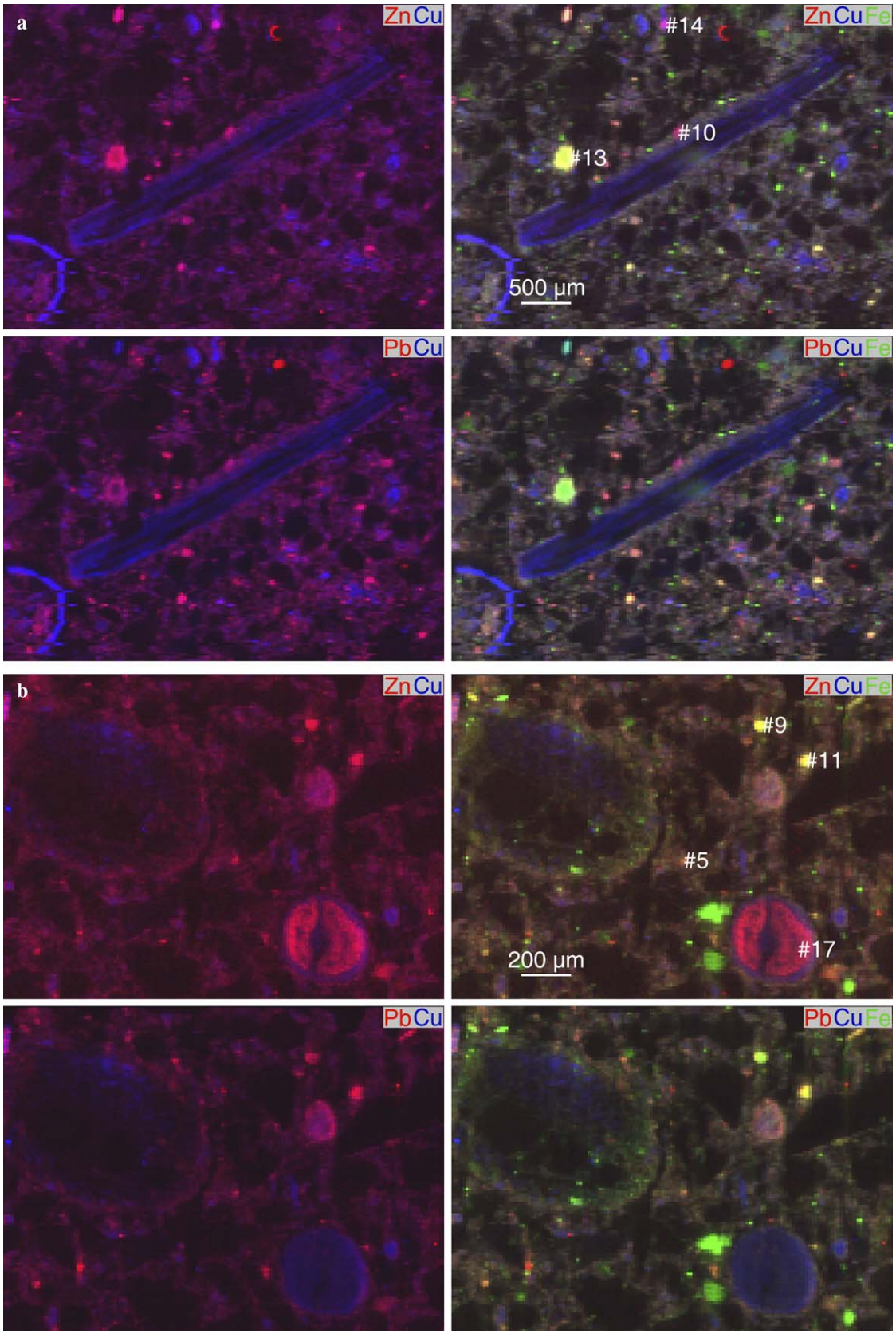

Fig. 2. Bicolor (left column) and tricolor (right column) µ-SXRF maps of the distribution of Zn and Pb (red), Cu (blue) and Fe (green) in two representative regions of two soil thin sections (a, b). The intensity of each color in each pixel is proportional to the concentration of the corresponding element. The overall brightness of a region is related to the sum of the concentrations, and the hue is related to the difference. The numbers indicate the spots where Zn K-edge µ-EXAFS spectra were collected. Steps of 20×20 µm, beam size = 16 (H) × 7 (V) μm^2 (FWHM).

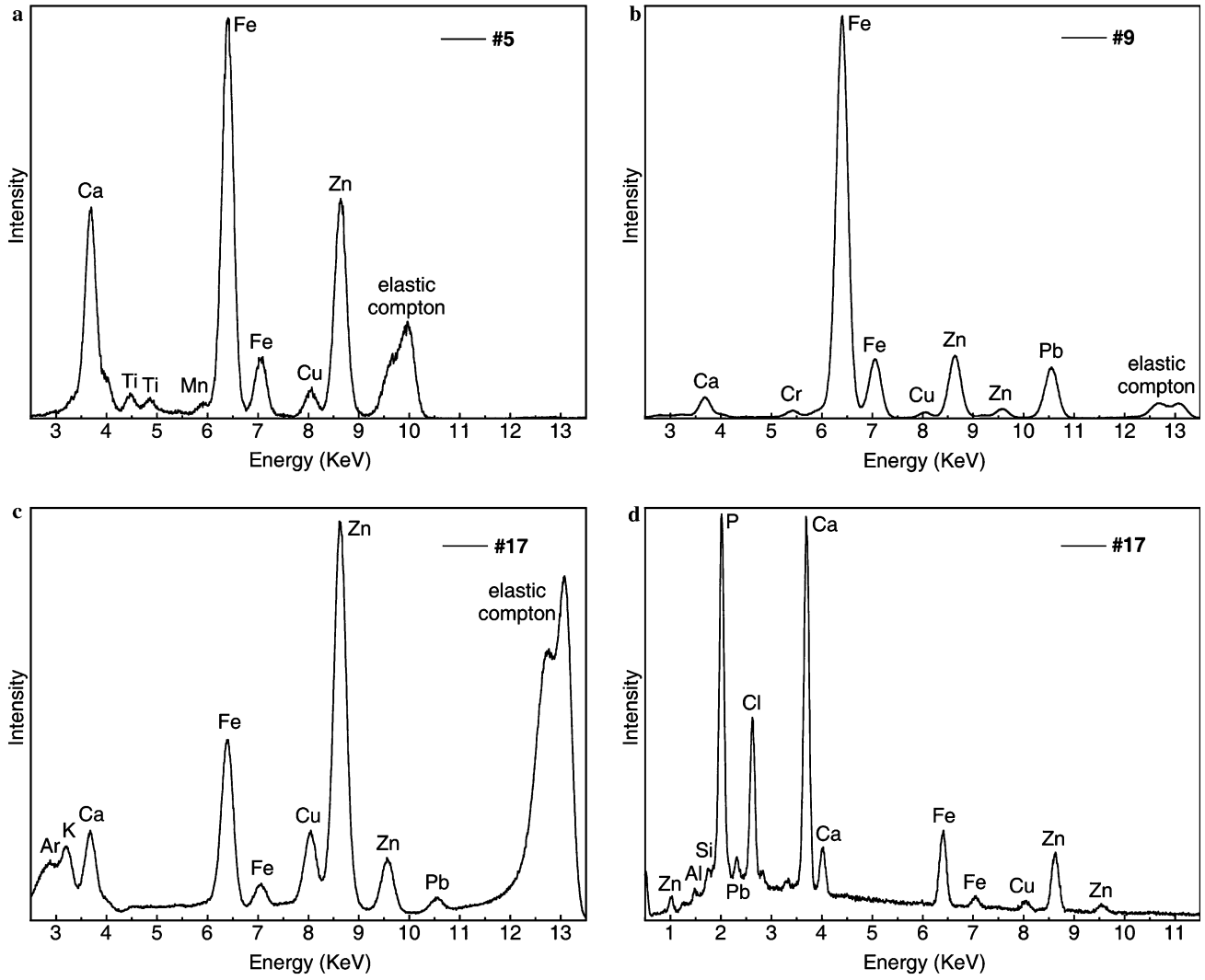

Fig. 3. Energy dispersive X-ray spectrometry (EDS) spectra collected with a microfocused X-ray source at POIs #5 (a), #9 (b) and #17 (c) from the elemental maps presented in Fig. 2, and EDS spectrum collected on a scanning electron microprobe at POI #17 (d). The Fe:Zn ratio appears closer to 1:1 through SEM compared to μ-SXRF analysis because measurements were performed in vacuum in SEM and air in μ-SXRF. Beam size = 5 (H) × 5 (V) μm^2 (FWHM).

contains major Ca and Cl, and minor Si, Al, and K. In contrast with Zn, whose distribution pattern resembled two half-moons, Cu was evenly distributed within the two half-moons (see the R(Pb)–B(Cu) map) and also in the central part of the grain and on its rim (see the R(Zn)–B(Cu) map). In R(Zn)–B(Cu) representation, the edge and the central regions appear purple because they contain some Zn, but only one fifth that of the half-moons. In contrast, the half-moons are reddish because the Cu signal is masked by the intense Zn signal ($Zn(K\alpha)_{moons}$:$Cu(K\alpha)_{moons}$ equal to 100:23). The uneven distribution of Cu and Zn suggests different speciation for the two metals. Two types of components were identified by SEM: organic cells with preserved shapes that are distributed homogeneously throughout the disk-shaped area, and microcrystalline minerals that occur interstitially between organic cells and form the skeleton of the two half-moon aggregates (Fig. 4). Therefore, we conclude from the μ-SXRF analysis and SEM observations that Cu is associated with the organic component, and Zn with the mineral component.

3.4. Nature of Zn species

On the basis of the μ-SXRF results, eighteen POIs (some of them are marked on the μ-SXRF maps in Fig. 2) were selected for Zn K-edge μ-EXAFS measurements. Of these spectra, 17 could be classified into two groups on the basis of their appearance (Fig. 5). The remaining spectrum, collected at a Zn 'hot spot' about 5 × 5 μm^2, was identical to that of gahnite ($ZnAl_2O_4$, Fig. 6). The spectra from the first group were collected in clay-rich areas, whereas those from the second group were collected in either Fe- or P-rich areas. The first set of spectra resembles that of Zn-containing kerolite $Si_4(Mg_{1.65}Zn_{1.35})O_{10}(OH)_2 \cdot nH_2O$ (ZnKer135), a trioctahedral phyllosilicate (Fig. 5a). The spectrum of ZnKer135 exhibits splitting of the first EXAFS oscillation at ~3.8 $Å^{-1}$, which is systematically observed when Zn is six-fold coordinated and its octahedron shares edges with those of 'light' elements (Mg or Al) as in some phyllosilicates, gibbsite, lithiophorite and hydroxy-Al interlayered 2:1 clay minerals (Manceau et al., 1987, 2000b, 2004, 2005; Scheinost

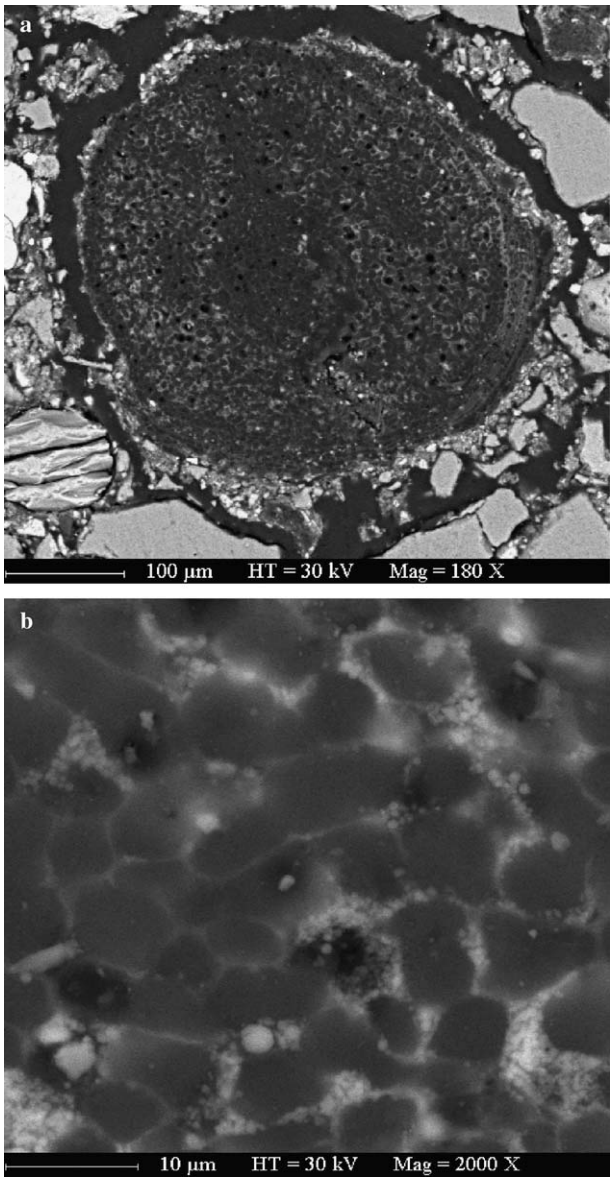

Fig. 4. Scanning electron micrographs of the 'coffee bean' area from the elemental map presented in Fig. 2b, at 180× (a) and 2000× (b) magnification. The higher magnification clearly shows a pseudomorphic texture containing biological cells and microcrystalline mineral precipitates. The lower magnification shows that the cells are homogeneously distributed in the grain, whereas the microcrystalline minerals form two half-moon aggregates.

et al., 2002). The nature of the host mineral will be determined below by PCA, but lithiophorite can be disregarded immediately because no Mn was detected. Although the spectra from #4 to #7 do not have their first EXAFS oscillation split, they were classified in this group because their third oscillation is halved in a similar manner as in kerolite. This series of spectra clearly contains at least two Zn forms, which may be either a phyllosilicate with a variable stoichiometry (i.e., varying amounts of 'heavy' and 'light' atoms in its octahedral sheet), or an unknown Zn species mixed with a single phyllosilicate.

The spectra of the second group have their first oscillation shifted to higher k values, relative to those from the first group (4.2 vs. 3.8 $Å^{-1}$), indicating that Zn is in tetrahedral coordination. These spectra also have lower amplitude, suggesting that Zn is surrounded by 'light' atoms or forms surface complexes. In agreement with the Zn–Fe and Zn–P chemical associations identified by µ-SXRF, an overall spectral similarity was observed between the unknowns of the second group and Zn-sorbed ferrihydrite (ZnFh) and Zn-containing phosphate (ZnPhos) (Fig. 5b). However, attempts to reconstruct the unknown spectra with a linear combination of ZnFh and ZnPhos failed, which suggests either that one of the two inferred species is invalid or that they are mixed with a third species.

PCA showed that the set of 17 multi-component µ-EXAFS spectra could be reduced to four orthogonal components, as indicated by the IND values (Table 5). Reconstruction of the 17 spectra with the first two, three, four, five, six, and seven components confirmed that the first four components were necessary to reproduce all experimental spectral features, and a trade-off in signal-to-noise ratio was observed between the fourth and fifth component. Therefore, the target transformation of the reference compounds from our database was performed in the orthogonal base of the four components. The quality of the transformation was examined visually and quantified by the residual R value between the original and the target-transformed reference spectra. Four families of Zn species were positively identified and retained as proxies: Zn-sorbed ferrihydrite (ZnFh), Zn phosphate dihydrate (ZnPhos), medium-Zn kerolite (ZnKer135), and willemite (Willem) (Fig. 7a).

Among the iron oxyhydroxides available in our database, Zn-sorbed ferrihydrite (ZnFh), in which Zn is fully tetrahedral (Waychunas et al., 2002; Trivedi et al., 2004), yielded the best reconstruction with lower R value ($R = 0.23$). The assumption of Zn-sorbed goethite (not shown) and Zn-substituted goethite (ZnGoet), in which Zn is octahedral, yielded poor reconstructions with R values equal to 0.72 and 0.74, respectively (Fig. 7b). In particular, the shape of the first oscillation for goethite was not correctly reproduced by the target transformation, because this region of the spectrum is sensitive to the $^{IV}Zn/^{VI}Zn$ ratio, with the frequency being left-shifted when the Zn-O distance increases (Schlegel et al., 1997). Of the various Zn phosphate references tested, Zn phosphate dihydrate ($Zn_3(PO_4)_2 \cdot 2H_2O$) yielded the best reconstruction ($R = 0.25$) (Fig. 7a). Other forms of Zn phosphate, including scholzite (not shown) and Zn-reacted hydroxyapatite (ZnApat), gave poorer reconstruction with $R = 0.68$ and $R = 0.77$, respectively (Fig. 7b).

Among the Zn phyllosilicate family of spectra, medium-Zn kerolite ($Si_4(Mg_{1.65}Zn_{1.35})O_{10}(OH)_2 \cdot nH_2O$, ZnKer135) gave the best spectral reconstruction ($R = 0.59$). The target testing of dioctahedral Zn–phyllosilicate, simulated here with the Zn-substituted montmorillonite from Redhill ([Zn] = 85 mg/kg) (ZnMont), was unsatisfactory ($R = 1.38$). Fig. 7 shows that the original and reconstructed

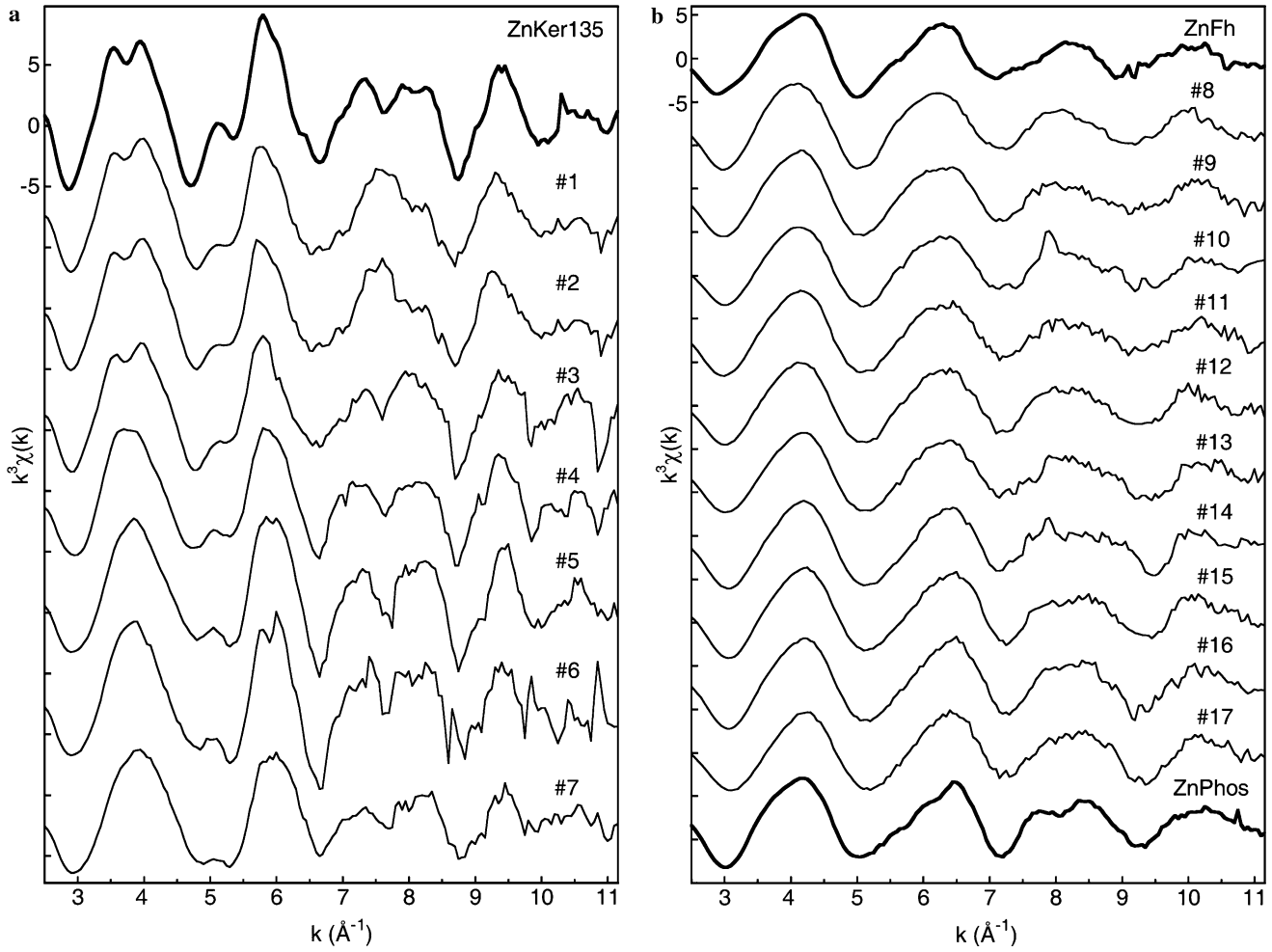

Fig. 5. Zn K-edge k^3-weighted μ-EXAFS spectra collected at different POIs of the two soil thin sections. Spectra are grouped in two populations according to their visual appearance, and compared with three reference spectra, (Zn,Mg)-containing kerolite (ZnKer135), in which Zn is octahedrally coordinated to oxygens (a), and Zn-sorbed ferrihydrite (ZnFh) and Zn phosphate (ZnPhos), in which Zn is tetrahedrally coordinated to oxygens (b).

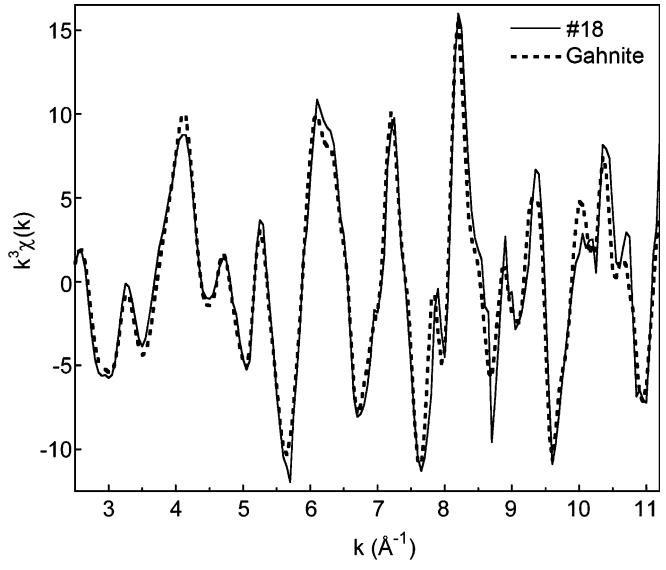

Fig. 6. Zn K-edge k^3-weighted μ-EXAFS spectrum collected at POI #18 (solid line) and its one-component fit to gahnite (dotted line).

Table 5
Output parameters from PCA

Component	Eigenvalue	IND[a]
1	120.0	0.0828
2	76.4	0.0423
3	23.8	0.0384
4	17.7	0.0360
5	11.1	0.0379
6	9.9	0.0402
7	8.4	0.0436

[a] Indicator value, for details see Manceau et al. (2002b).

spectra for ZnMont differed in shape and in phase in the 5–9 $Å^{-1}$ k-interval, whereas good agreement was obtained with the medium-Zn (ZnKer135) trioctahedral kerolite reference. This suggests that Zn has a trioctahedral local environment in the phyllosilicate species, as often observed in soils and sediments (Isaure et al., 2005; Panfili et al., 2005). The average stoichiometry of the soil Zn phyllosilicate was estimated by testing several kerolite refer-

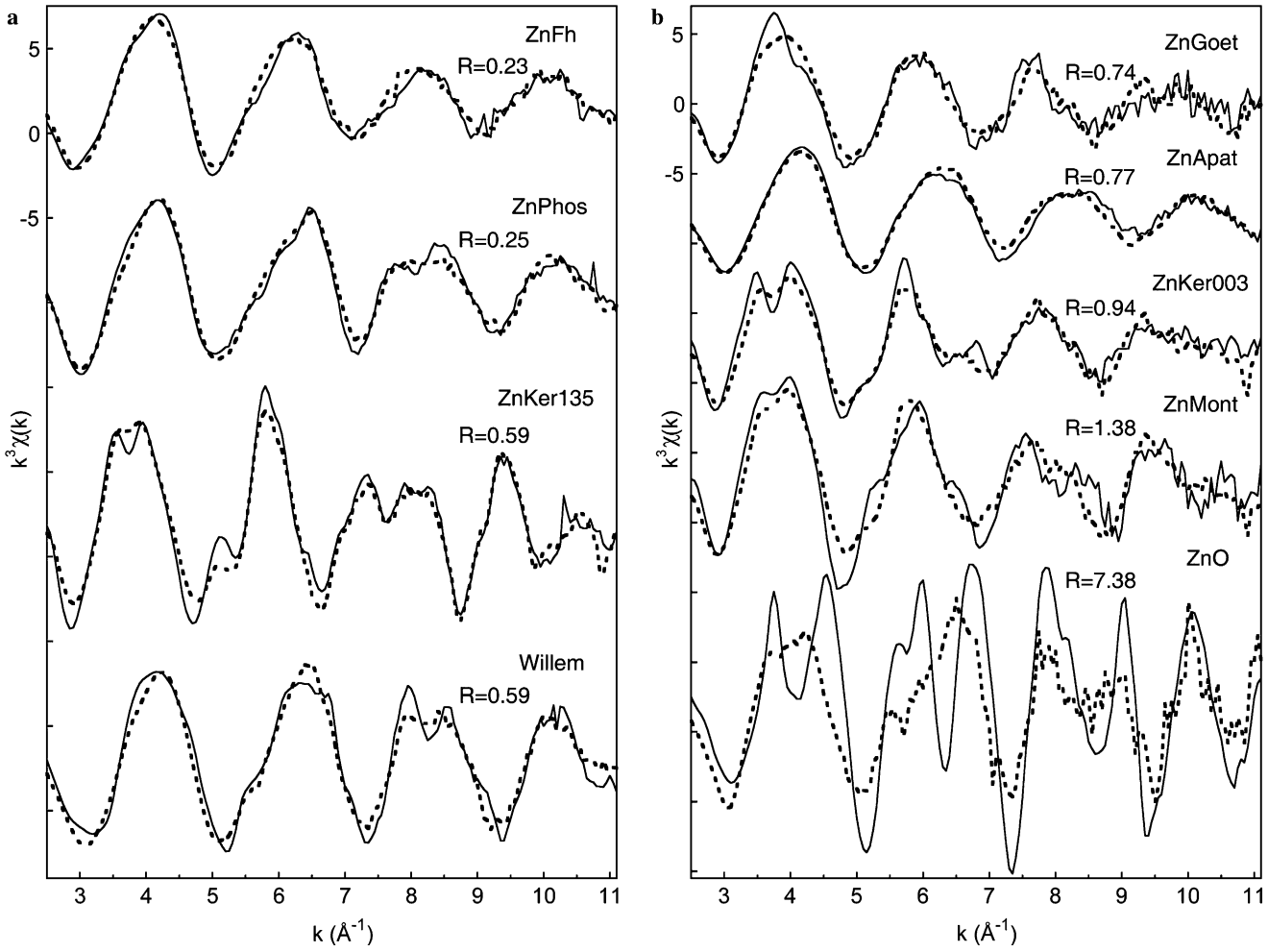

Fig. 7. Zn K-edge k^3-weighted EXAFS spectra and target transformations of a selection of Zn reference compounds. The quality of the transformation is evaluated by the residual R value between the original reference spectrum (solid line) and the target transformed spectrum (dotted line). (a) Zn-sorbed ferrihydrite (ZnFh), Zn phosphate dihydrate (ZnPhos), medium-Zn kerolite (ZnKer135), and willemite (Willem) are statistically the most likely Zn species. (b) Zn-substituted goethite (ZnGoet), Zn-reacted hydroxyapatite (ZnApat), low-Zn kerolite (ZnKer003), Zn-substituted montmorillonite (ZnMont) and zincite (ZnO) are discriminated from the four likely species in a statistically meaningful way.

ences with various Zn/Mg ratios. The reconstruction was poor with the pure-Zn end-member ($Si_4Zn_3O_{10}(OH)_2 \cdot n$-$H_2O$, data not shown, $R = 0.81$), and worse with the low-Zn end-member ($Si_4Zn_{0.03}Mg_{2.97}O_{10}(OH)_2 \cdot nH_2O$, ZnKer003, $R = 0.94$). We note that, in contrast to the dioctahedral reference, the original and reconstructed spectra for the trioctahedral hydrous silicate references were always in phase over the experimental k interval, independently of their Zn/Mg ratio, strengthening the improbability of montmorillonite as a possible Zn species. The possibility of a Zn surface complex on the edges of phyllosilicate layers was discarded by testing Zn-sorbed hectorite ($R = 1.18$, data not shown) (Schlegel et al., 2001a,b). Other tested layered Zn species include (Zn,Al)-hydrotalcite and hydroxy-Al interlayered phyllosilicate, but the obtained R values were in the same high range as montmorillonite (1.28 and 1.39, respectively) (data not shown).

The fourth and last identified species is willemite, an anhydrous Zn silicate (Zn_2SiO_4, $R = 0.59$). The spectrum of this species has a characteristic sharp-pointed resonance at 8 $Å^{-1}$ (Fig. 7a), which can be used to ascertain its presence in a mixture, as observed in Fig. 5b for the spectra collected at POIs #10 and #14. A number of other Zn species previously identified or inferred in contaminated soils and sediments, including minerals such as zincite (Fig. 7b), sphalerite, franklinite, organic Zn complex with humic and low-molecular-weight organic acids (Isaure et al., 2002; Sarret et al., 2004; Panfili et al., 2005) were tested and led to poor reproduction of the data, which indicates that these species are not present in significant amount in the studied soil (i.e., <5–10% of total Zn, depending on the reference). In summary, four Zn species were identified by PCA, Zn-sorbed ferrihydrite, Zn phosphate, medium-Zn kerolite, and willemite, in addition to gahnite identified in a hot spot.

The nature and proportion of the Zn species at each POI was determined next by LCF of the 17 multi-component μ-EXAFS spectra to the five identified Zn species. The sensitivity of this approach is illustrated below with three spectra, one from the clayey matrix (POI #5), one

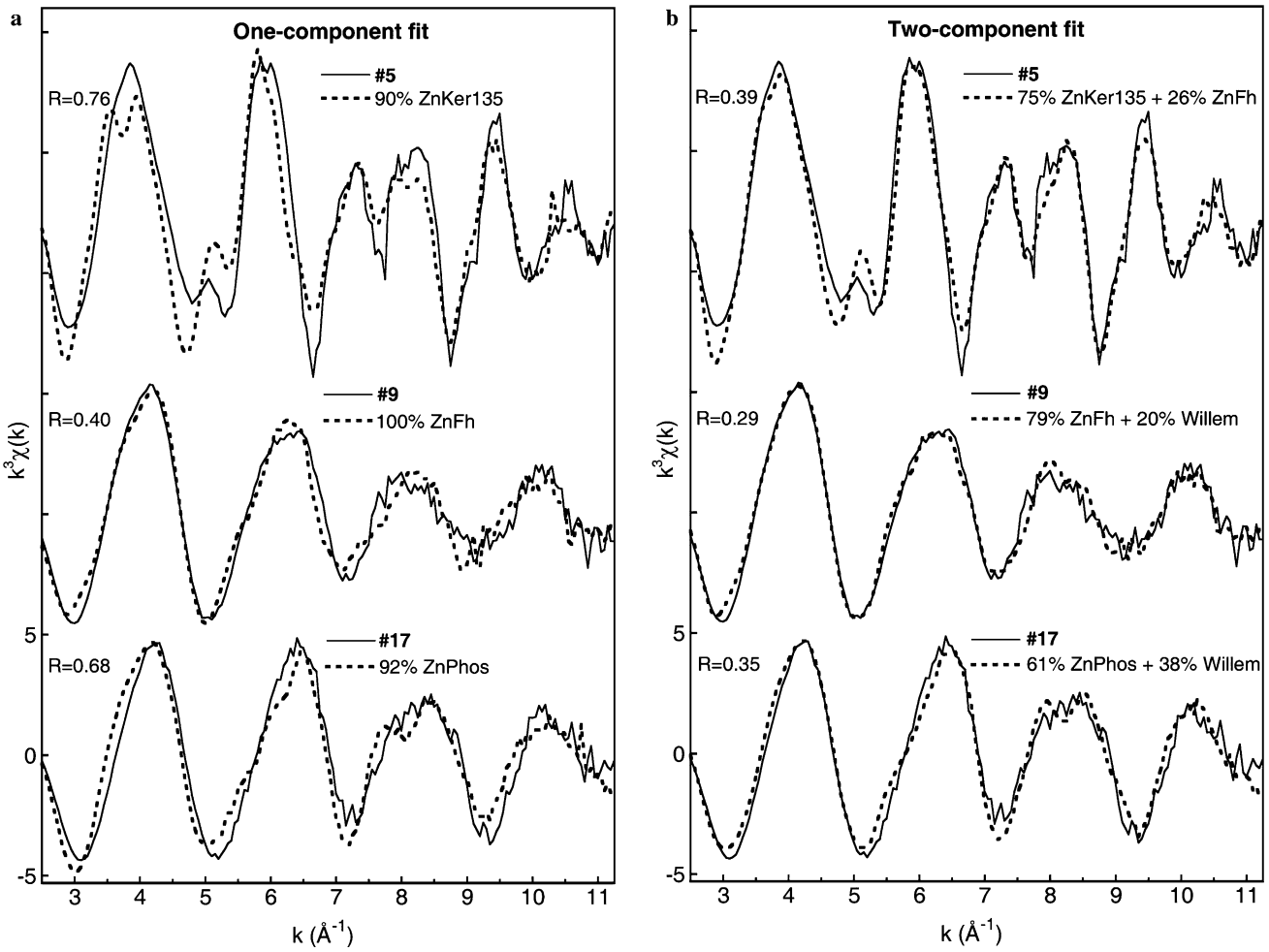

Fig. 8. Zn K-edge k^3-weighted μ-EXAFS spectra (solid line) collected at POIs #5, #9 and #17, and their best one- (a) and two-component (b) fits (dotted line).

from an Fe-rich area (POI #9), and one from a P-rich area (POI #17) (Fig. 8). The one-component fit to spectrum #5 identified medium-Zn kerolite as the most likely species ($R = 0.76$). Adding Zn ferrihydrite significantly improved the fit as indicated by the 48% decrease in R ($R = 0.39$). Zn ferrihydrite was often detected together with Zn phyllosilicate, presumably because of its nanodivided nature and its frequent occurrence as 'background' species in soil matrices (Hochella et al., 1999; Manceau et al., 2002b). This species is probably responsible for the brownish cast of the two μ-SXRF maps in RGB representation (Fig. 2). The one-component fit to spectrum #9 identified Zn ferrihydrite as the most likely major Zn species at this spot ($R = 0.40$), in keeping with the high Zn–Fe correlation measured by μ-SXRF. A two-component fit was attempted, and the assumption of a mixture of 79% Zn ferrihydrite and 20% willemite decreased R by 28% ($R = 0.29$). The one-component fit to spectrum #17 identified Zn phosphate, in agreement with the Zn–P correlation at this point. Adding willemite in a two-component fit improved the spectral match and reduced R by 48%. For the three spectra shown in Fig. 8, the proportion of the third phase obtained with three-component fits was <10% and, thus, was considered insignificant enough to only consider two-component combinations. In particular, no layer double hydroxide (LDH) was detected at POI #5, which is consistent with the transformation of this species into phyllosilicate with time (Voegelin et al., 2005).

In summary, all multi-component μ-EXAFS spectra presented in Fig. 5 were fitted successfully to linear combinations of only two components taken from the set of the four Zn species identified by PCA: ferrihydrite, phosphate, phyllosilicate, and willemite. Gahnite was found in one Zn 'hot spot,' and never in a mixture with other Zn species at the analyzed POIs.

3.5. Quantitative speciation of Zn in the untreated soil

The fractional amounts of each Zn species in the soil were determined by LCF of the EXAFS spectrum of the powdered soil sample to linear combinations of the EXAFS spectra of the five identified Zn species. The powder EXAFS spectrum (noted ×0) looks intermediate in phase,

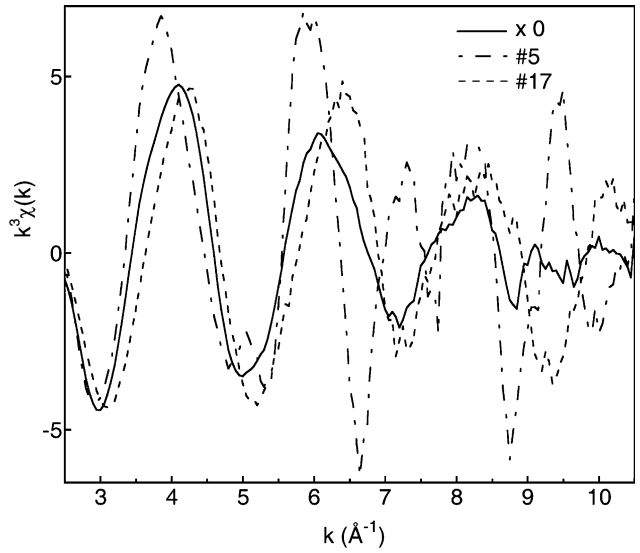

Fig. 9. Zn K-edge k^3-weighted powder EXAFS spectrum of the bulk soil (×0) together with the two μ-EXAFS spectra collected at POIs #5 and #17.

shape and amplitude to the two μ-EXAFS spectra collected at POIs #5 and #17 (Fig. 9). To a first approximation, the three spectra seem to belong to a pseudobinary system, in which one end-member is spectrum #5 (mixture of 75% Zn kerolite and 26% Zn ferrihydrite) and the other is spectrum #17 (mixture of 61% Zn phosphate and 38% willemite). However, the bulk soil spectrum could not be described quantitatively by a linear combination of the two two-component spectra, according to $\alpha \cdot (0.75\text{ZnKer} + 0.26\text{ZnFh}) + (1-\alpha) \cdot (0.61\text{ZnPhos} + 0.38\text{Will})$. If this were the case, then the ×0, #5 and #17 spectra would all intersect at the same points, called isosbestic points (Manceau et al., 1998), which is clearly not the case, for example at 4.9, 5.4, and 9.0 Å^{-1}. This means that the ratio of ZnKer to ZnFh, and of ZnPhos to Willem measured at POIs #5 and #17 are not constant throughout the powdered sample. The lower amplitude of the powder spectrum relative to the two μ-EXAFS spectra results from the higher multiplicity of the Zn structural environments in the soil volume, thereby justifying multiple-species fits. Results from the LCF indicated that Zn ferrihydrite, Zn phosphate and Zn kerolite are predominant, because omitting any of these species significantly degraded the quality of the simulation (Fig. 10). Adding willemite in a four-component fit improved the spectral match and decreased the R by 17%, the best statistical agreement being obtained with a mixture of 30% Zn ferrihydrite, 28% Zn phosphate, 24% medium-Zn kerolite, and 11% willemite ($R = 0.19$). Ten percent of willemite in the four-component fit corresponds to the generally accepted detection limit of metal species by this linear least-squares combination fit analysis of EXAFS spectra (Manceau et al., 1996; Ostergren et al., 1999; O'Day et al., 2000; Isaure et al., 2002). Gahnite represents less than 10% of total Zn, because adding this component did not significantly improve the spectral simulation.

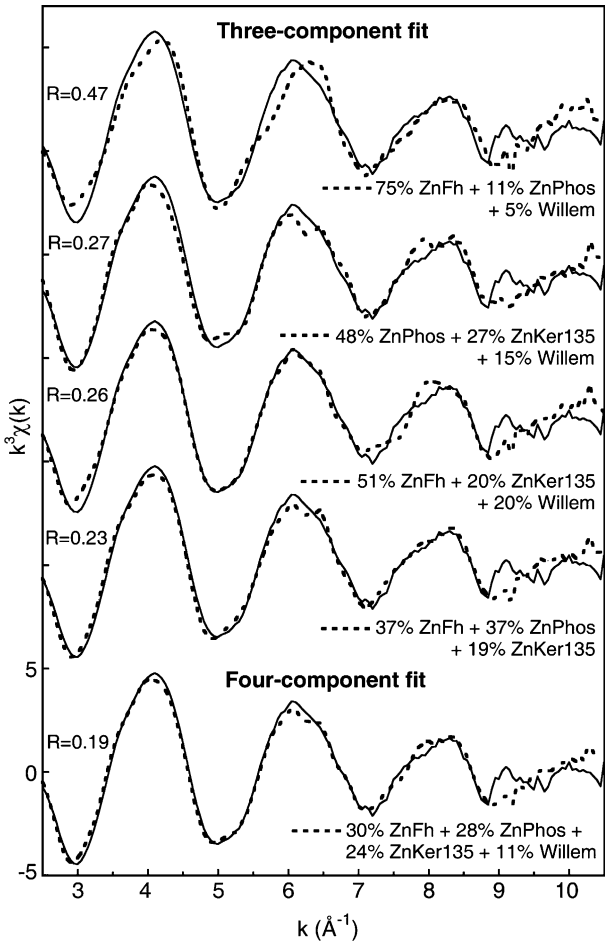

Fig. 10. Zn K-edge k^3-weighted EXAFS spectrum of the powdered soil sample (solid line) with three and four-component least-squares fits to linear combination of reference spectra (dotted line). The bulk soil spectrum is best simulated ($R = 0.19$) with a mixture of 30% Zn-sorbed ferrihydrite, 28% Zn phosphate, 24% medium-Zn kerolite, and 11% willemite (estimated accuracy ±10% of the total zinc). Gahnite, firmly identified by μ-EXAFS, represents less than 10% of the total Zn, because adding this component did not significantly improve the spectral simulation.

3.6. Quantitative speciation of Zn in the soil after chemical treatments

In the following, the effect of citrate, EDDS, and EDTA treatments on the forms of zinc in the soil is examined. Fig. 11 shows the Zn K-edge powder EXAFS spectra of the soil before (×0) and after 24 h treatment with citrate (×Ci), EDDS (×EDDS) and EDTA (×EDTA), together with the reference spectra of the four major Zn species initially present in the soil. The three chemical treatments modified the shape of the second and third EXAFS oscillations in a similar manner, rendering them more symmetrical than they were initially in ×0. In particular, the doublet of the third oscillation, which is marked in ZnPhos (black arrows in Fig. 11), and still apparent in ×0, has disappeared. Concomitantly, two shoulders on the left tail of the second oscillation are noticeable after treatment (semi-black arrows in Fig. 11). These spectral changes, added to the fact that the three

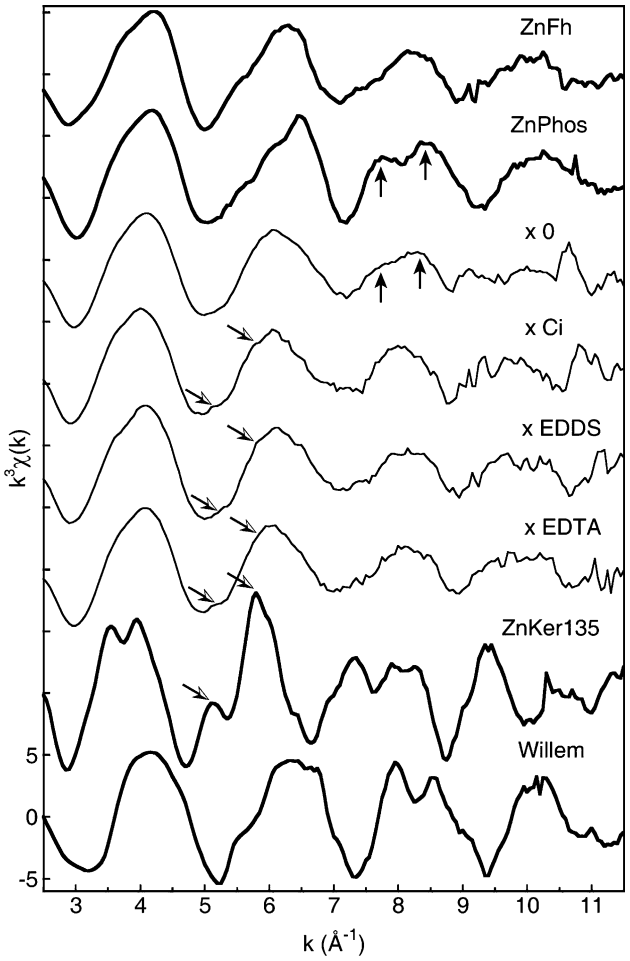

Fig. 11. Zn K-edge k^3-weighted EXAFS spectra of the powdered samples for the untreated soil (×0) and the residuals after 24 h contact time with citrate (×Ci), EDDS (×EDDS), and EDTA (×EDTA), together with the reference spectra of the major Zn species identified in the untreated soil.

extractants removed about the same amount of Zn (citrate 43%, EDDS 42%, and EDTA 40%), suggest that the Zn phosphate species was dissolved preferentially after 24 h, thereby increasing the proportions of remaining species in the treated soil fractions. To confirm this hypothesis and quantify the speciation of Zn in the treated soil, the spectra of the treated soil were fitted by linear combination of the five Zn species. The one-, two-, and three-component fits of the treated and untreated soils are shown in Fig. 12, and the fractions of each component are given in Table 6. Best one-component fits were obtained with Zn ferrihydrite, then Zn kerolite was revealed as the second most likely species, and finally willemite as the third species. The three-component model yielded the best fit for the three treated soil fractions, as indicated by R values and the closeness to 100% of the sum of all species. Adding Zn phosphate as a fourth component did not improve significantly the fits, in contrast to the spectrum of the untreated soil (×0). For this last sample, adding Zn phosphate decreased the R value by 27% (Table 6).

Zn phosphate, which amounted to $28 \pm 10\%$ of total Zn in the untreated soil, is below the detection limit in the three treated samples, which indicates that it was dissolved preferentially. The mole fraction of Zn kerolite slightly increased from ~24% in the untreated soil to ~29 to 30% in the treated soil. Because of the high-amplitude and multiple-frequency shape of this reference spectrum, its contribution to the total EXAFS signal became visible after treatment, as seen by the appearance of the two shoulders on the left side of the second oscillation, which are reminiscent of the two shape resonances of the kerolite spectrum at 5.2 and 5.8 Å^{-1}. The relative proportion of willemite remained almost constant after citrate and EDDS treatment, but increased by ~6% with EDTA.

Some zinc liberated by phosphate dissolution may have been readsorbed on other phases. To test this, the fractional amount of each Zn species after treatment was compared to the fractional amount of each Zn species before treatment. Results reported in Fig. 13 show that the proportions of Zn species are, within precision, the same in the treated and untreated samples: ~30% Zn ferrihydrite, ~24% Zn kerolite, and ~11% willemite. Another way to look at the data is to compare the fractional amount of Zn phosphate in the untreated soil ($28 \pm 10\%$) and the difference to 100% (or 93% if using experimental values in Table 6) of the sum of the normalized proportions of each species in the treated soil (~40%). These two values are conservative, which means that the amount of dissolved Zn is the same as the amount of Zn phosphate in the native soil. This Zn phosphate pool is the most labile in the presence of complexing organic compounds, and is solubilized with a good selectivity since no reagents seem to have modified significantly the proportions of Zn ferrihydrite, Zn kerolite, and willemite.

Dissolution of Zn phosphate was confirmed by the Zn and P concentrations in the extracted solutions (Fig. 14a). The dissolved Zn/P molar ratio was 1.0 with EDDS and 1.5 with EDTA, similar to the ratio in Zn phosphate dihydrate (Zn/P = 1.5), the model compound used as a proxy for the family of Zn phosphate minerals. This ratio was 0.4 with citrate, suggesting that this organic molecule extracted other P-containing phases. If the Zn/P molar ratio of the citrate-extracted Zn phosphate is 1.5, then about 6% of the 24% P extracted with citrate was bound to Zn. The other 18% P ought to be bound to other dissolved cations. This inference is consistent with the analysis of dissolved Fe and Ca, since citrate extracted more Fe (11%) than EDDS (4%) and EDTA (0.5%) and, above all, more Ca (28 vs. 2 and 4%, respectively) (Fig. 14b). The possible co-dissolution of Zn-, Ca- and Fe-containing phosphates by citrate is consistent with its lack of selectivity for heavy metals, as discussed in Section 4.2.3.

In summary, the combination of chemical extractions with quantitative EXAFS analysis revealed that citrate, EDDS, and EDTA selectively dissolved Zn phosphate after 24 h of treatment, and were essentially inert during

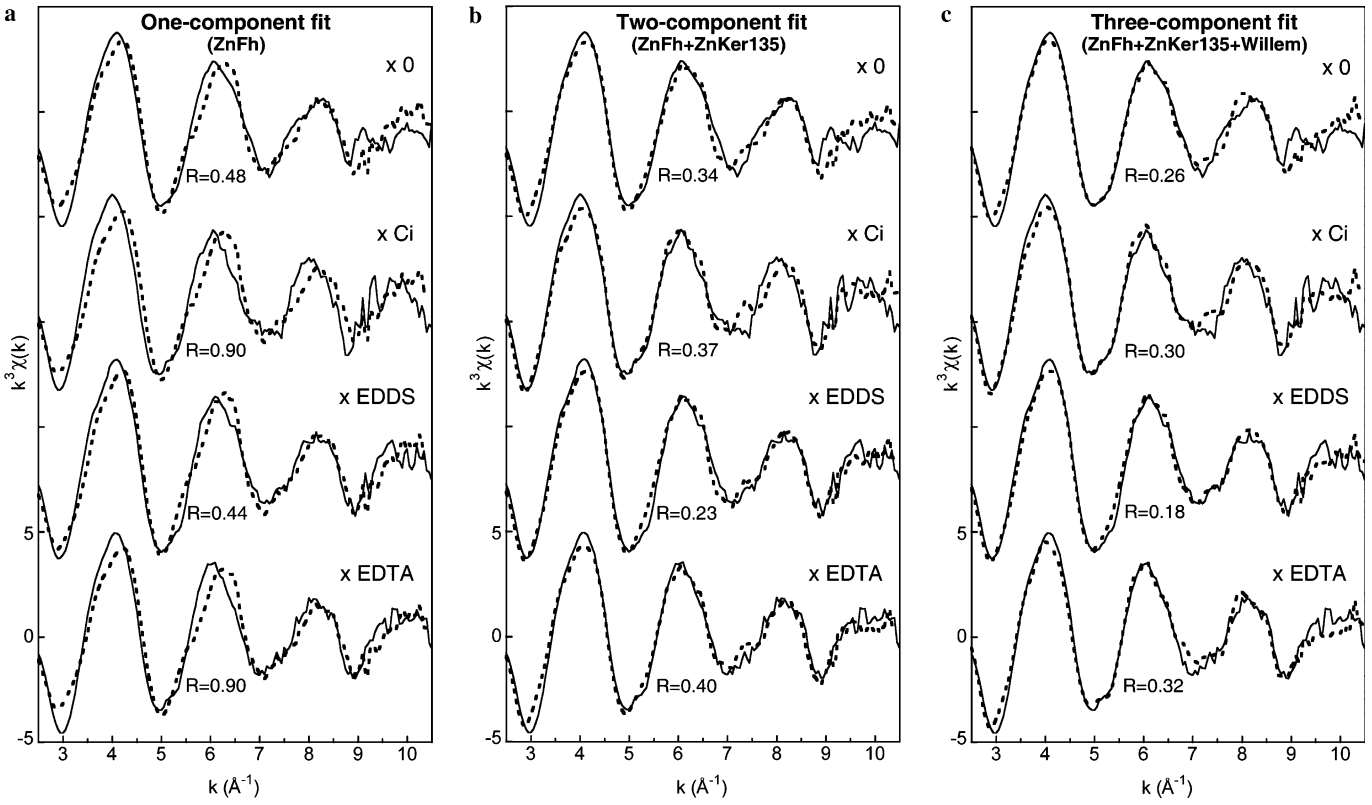

Fig. 12. Zn K-edge k^3-weighted EXAFS spectra of the untreated soil (×0) and of the treated fractions after 24 h contact time with citrate (×Ci), EDDS (×EDDS) and EDTA (×EDTA) (solid lines), together with one-, two-, and three-component fits (dotted line) using Zn-sorbed ferrihydrite (a), plus medium-Zn kerolite (b), and plus willemite (c). The fractions of each component are listed in Table 6. The residual R value was minimum and the sum of Zn species was close to 100% with the three-components model (Zn-sorbed ferrihydrite + medium-Zn kerolite + willemite) for the three treated fractions (×Ci, ×EDDS, ×EDTA). Adding Zn phosphate as fourth component did not improve significantly the spectral fits, in contrast to the spectrum of the untreated soil (×0), which is best fitted with a four-components model (Zn-sorbed ferrihydrite + medium-Zn kerolite + willemite + Zn phosphate) (see Fig. 10). The sum of all fractions equals 93% in each case, confirming that the number of species included in the fit is reasonable.

Table 6
Relative proportions of Zn species determined by LCF

Sample	Number of components	ZnFh (%)	ZnKer135 (%)	Willem (%)	ZnPhos (%)	Sum (%)	R
×0	1	86				86	0.48
	2	78	13			91	0.34
	3	51	20	20		91	0.26
	4	30	24	11	28	93	0.19
×Ci	1	84				84	0.90
	2	68	24			92	0.37
	3	52	29	12		93	0.30
×EDDS	1	92				92	0.44
	2	76	16			92	0.23
	3	54	29	10		93	0.18
×EDTA	1	84				84	0.90
	2	70	22			92	0.40
	3	46	30	17		93	0.32

this reaction time with respect to Zn ferrihydrite, phyllosilicate and willemite, the three other major forms of Zn in the soil. The reasons for the higher solubility of Zn phosphate to the three extractants are discussed below.

4. Discussion

4.1. Original Zn speciation in soil

Five Zn-bearing minerals were identified in this study: Fe oxyhydroxide, phosphate, phyllosilicate, willemite, and gahnite, in proportions of ~30, 28, 24, 11, and less than 10%, respectively. About 80% of Zn is associated with hydroxylated secondary minerals, and the remainder with dehydroxylated (i.e., willemite and gahnite), and probably primary in origin, minerals. Despite the high organic content of the soil, no organic forms of Zn were detected. Thus, the mobility of Zn in the original soil under real field conditions is controlled mostly by the formation of secondary minerals.

Zn-sorbed Fe oxyhydroxide is the first of the major forms of Zn in the soil, and was modeled with ^{IV}Zn-sorbed ferrihydrite. Although we have no direct evidence for this species (i.e., it was always mixed with other species), our finding is supported by three arguments. First, the target testing revealed that Zn in the soil iron oxyhydroxide aggregates was tetrahedral, which allows us to dismiss the occurrence of Zn-sorbed or substituted into crystalline Fe

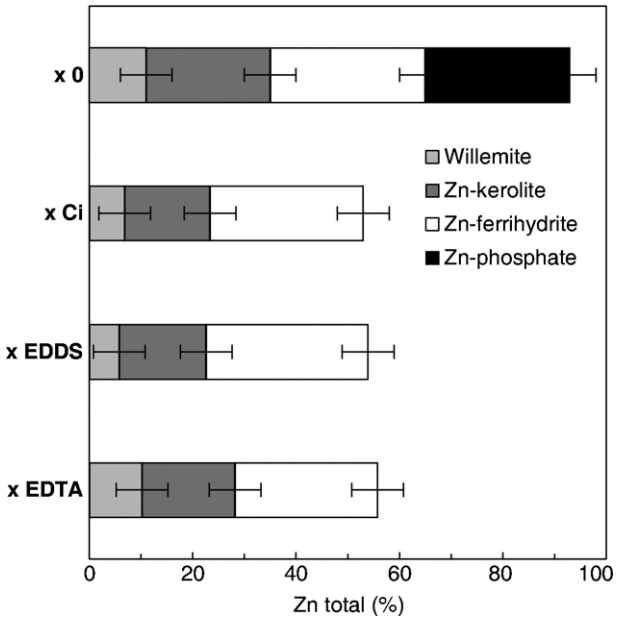

Fig. 13. Mole fractions of Zn species in the soil before (×0) and after 24 h chemical treatment with citrate (×Ci), EDDS (×EDDS), and EDTA (×EDTA). Values for the treated samples were normalized to the sum of Zn species in the untreated soil (i.e., 93% of total initial Zn). The uncertainty is estimated to ±10% of total zinc. The results clearly show that the Zn phosphate species is absent in the three treated soil fractions, and that the fractional amount of the three other species is conservative among all samples, meaning that the chelating agents selectively dissolved the Zn phosphate component species.

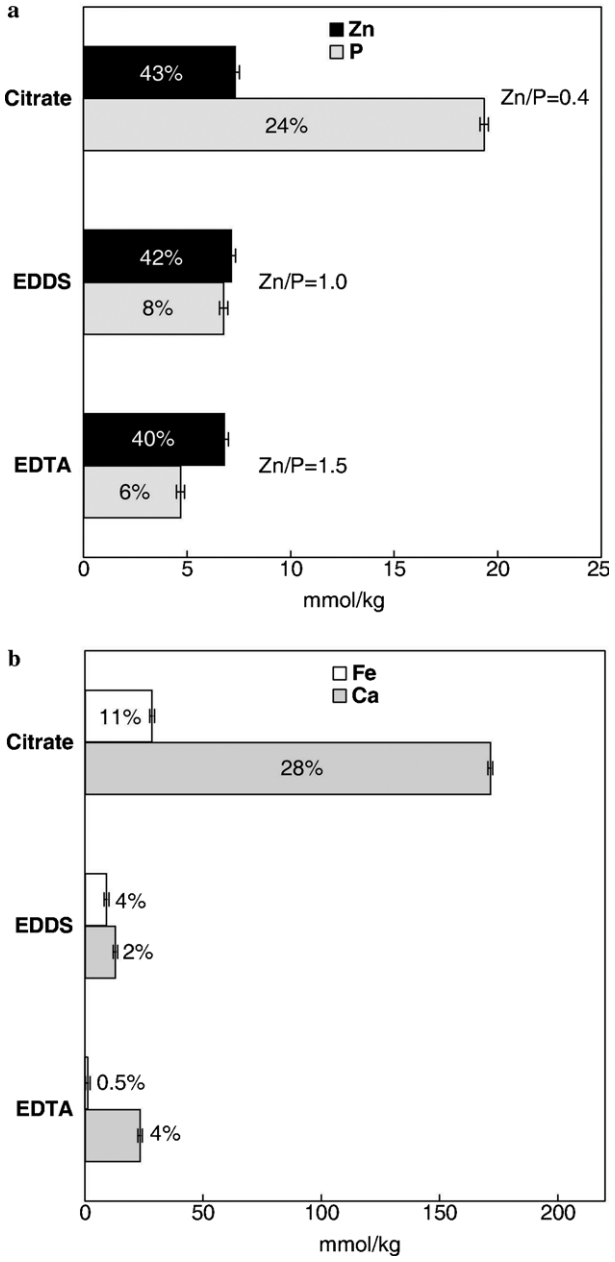

Fig. 14. Aqueous concentration of Zn and P (a), and Fe and Ca (b) in the extraction solution after 24 h of reaction time with citrate, EDDS and EDTA. Error bars indicate the deviation from duplicates. The percentages correspond to the weight fractions of the extracted elements. The Zn/P molar ratios in the extracted solutions also are indicated.

oxyhydroxides, as Zn is octahedral in these species. Second, the low amplitude of the EXAFS signal indicated that the structural order around Zn is limited to a few atomic shells, which suggests that Zn forms a surface complex of the type found on ferrihydrite. Third, the association of Zn with Fe oxyhydroxide was pervasive, because it was detected everywhere throughout the soil matrix mixed with other minerals, either as coatings on willemite and phosphate grains, or as aggregates in association with phyllosilicate in the finely divided matrix. Similar results were reported by Manceau et al. (2002b), who contended that, owing to its nanophase nature, ferrihydrite occurs as a 'background' species consistently throughout soil matrices. Therefore, the tetrahedral coordination of Zn in association with iron oxyhydroxide in the soil, the pervasive distribution of this constituent and the high metal sorption capacity of ferrihydrite in general (Davis and Kent, 1990; Spadini et al., 1994; Cornell and Schwertmann, 1996; Hochella et al., 1999), all support Zn-sorbed ferrihydrite as the most likely Zn-containing ferric phase in the soil.

Zn phosphate, modeled here with Zn phosphate dihydrate, is the second major form of Zn. Its occurrence was determined unambiguously by μ-EXAFS and supported by SEM-EDS. Zn phosphate was observed previously in a contaminated soil amended with phosphate, and on the root surface of *Agrostis tenuis* grown on this amended soil (Cotter-Howells and Caporn, 1996), and also in a P-rich Zn-contaminated sediment vegetated by graminaceous plants (*Agrostis tenuis* and *Festuca rubra*) (Panfili et al., 2005). Consequently, the occurrence of this species in our highly fertilized agricultural soil is not surprising especially with respect to the elevated phosphorus content ($[P_2O_5] = 0.6\%$) and excess of zinc ($[Zn] = 1103$ mg/kg). The exact nature of Zn bound in the phosphate phase could not be established precisely, but the featured shape of its EXAFS spectrum suggests that this phase is relatively crystalline. Our results also suggest that this form is inorganic.

Zn-containing phyllosilicate is the third major form of Zn. Its trioctahedral nature was established by target

transformation. The high amplitude of the EXAFS signal from this species is a strong indication that Zn is incorporated in the phyllosilicate structure, and does not form a surface complex on layer edges. This result, together with the fact that the octahedral sheets contain on average about as many Zn as Mg atoms, suggests that Zn did not sorb on the surface of preexisting phyllosilicate particles, but instead that this species resulted from the coprecipitation of dissolved zinc and silica. This hypothesis is consistent with the sandy nature of the soil ($[SiO_2] = 79.6\%$, and 69 wt.% of sand fraction), since phyllosilicate readily precipitates when a dissolved metal is in contact with quartz and silica (Manceau et al., 1999), and also with the low amount of phyllosilicate surface sites available for metal sorption, since the soil does not contain many clay minerals (8 wt.%). Zn-containing trioctahedral phyllosilicate is a common species in soils and oxidized sediments at circumneutral pH, and is a prevalent form of zinc in low-temperature continental settings in temperate climates (Manceau et al., 2000a; Isaure et al., 2002, 2005; Panfili et al., 2005). Here, this species takes up about a quarter of the total molar Zn content.

Willemite (Zn_2SiO_4) is the fourth Zn-species in abundance. It is an anhydrous silicate, which nominally forms at high temperature and, consequently, has been frequently observed in soils and sediments affected by smelting processes (Thiry and Van Oort, 1999; Manceau et al., 2000a; Isaure et al., 2002; Thiry et al., 2002). In this study, the source of willemite is presumably also anthropogenic, and may result either from irrigation with wastewater containing smelter dust particles or from atmospheric fallout. The latter source is most likely since the Pierrelaye land is located near an industrialized area from the Paris suburb. This hypothesis was tested by measuring the heavy metal content in a soil under permanent forest located near the agricultural land of Pierrelaye (Baize et al., 2002). The measured concentrations of Zn (87 mg/kg), Pb (114 mg/kg), and Cu (28 mg/kg) were much lower than in the irrigated fields (Zn 150–3150 mg/kg, Pb 80–668 mg/kg, and Cu 50–390 mg/kg), but still higher than the estimated geochemical background (Zn 7 mg/kg, Pb 7 mg/kg, and Cu 3 mg/kg), therefore suggesting the possibility of an atmospheric input for willemite. Willemite was identified by μ-EXAFS in association with Zn ferrihydrite and Zn phosphate, but not with Zn phyllosilicate. The primary zinc silicate grains of willemite may act as a physical support for the precipitation of the two secondary Zn minerals, but not as a chemically reactive substrate because the weathering of willemite is expected to promote the formation of hydrous sheet silicate.

Gahnite ($ZnAl_2O_4$), the last of the five species identified in this study, was detected only by μ-EXAFS and was below the detection limit of powder EXAFS (~10%). Gahnite is a Zn spinel typically formed in high temperature metamorphic environments (Hochella et al., 1999). Consistently with the usual natural occurrence of this mineral, anthropogenic gahnite has been described in soils and sediments affected by atmospheric fallout of Zn dusts emitted by smelting activities (Thiry et al., 2002; Isaure et al., 2005; Panfili et al., 2005). However, gahnite was also found in an acid mine drainage site (Hochella et al., 1999), and was reported to form in the laboratory at low temperature during ferrihydrite breakdown reactions in the presence of high concentrations of metals (Cornell, 1988). In this study, gahnite was found fortuitously in a micrometer-sized Zn hot spot, and this observation, together with the concomitance of willemite, lends support to its anthropogenic origin.

4.2. Mechanism of metal solubilization by chelants

4.2.1. EDTA

EDTA strongly binds multivalent cations (MVCs), such as Ca^{2+}, Al^{3+}, Fe^{3+}, Cu^{2+}, Zn^{2+}, and Pb^{2+} (Table 2). For example, equilibrium thermodynamic calculations show that MVC-containing minerals, such as calcite, ferrihydrite, hydroxylapatite, hopeite, smithsonite, and cerussite, are completely dissolved below pH 9 in contact with 1% excess EDTA (or EDDS), i.e., when the ligand concentration is 1% higher than the total concentration of MVCs in the solid phase. This is because the activity of the free (uncomplexed) ligand decreases the activities of MVCs below the solubility limit of the solid. In our dissolution experiments, it is important to know whether the complexation of MVCs consumed all of the EDTA, because this information provides insight on the main chemical process responsible for the solubilization of metals. If free ligands were present in the suspension, then the extraction of MVCs was kinetically driven, and time-resolved measurements of the aqueous concentration of MVCs can be regarded as representative of the apparent dissolution rate constants of the solid phase(s). If the ligand were totally saturated with MVCs, then one or several MVC-containing phases dissolved rapidly, and values of $[MVC]_{aq}$ were in equilibrium with the MVC-supplying phase(s). In this case, the nature of the dissolving phase(s) can be predicted from solubility constants, MVC hydrolysis constants, and ligand–MVC complexation constants. However, this approach requires that the unknown MVC-supplying phases and chemical processes, such as complexation with competing ligands, desorption, and cation exchange, are not significant. These other processes can be ignored at high [ligand]/[solid] concentration ratios, particularly in our cycling experiments, since the chelant was repeatedly renewed.

In the cycling EDTA extraction experiment, 200 g/L solid was exposed five times for 24 h each time to fresh 7 mmol/L Na_2H_2EDTA. The sum of the MVCs concentrations ($\Sigma[MVC]$) in the supernatant was nearly constant (i.e., 6.58–7.12 mmol/L, Table 4) in each of the first four cycles, which suggests that the EDTA ligand was saturated with MVCs each time, and thus that dissolution occurred at equilibrium with respect to the solid phases. Ca was the predominant MVC leachate, and its aqueous concentration increased from 4.67 mmol/L in the 1st cycle to

6.41 mmol/L in the 4th cycle. $[Zn]_{aq}$, $[Pb]_{aq}$, and $[Cu]_{aq}$ concomitantly decreased, but not enough to compensate the Ca variation; so the $[Ca]_{aq}$ to Σ[MVC] ratio increased from 66% in the 1st cycle to 92% in the 4th cycle. This indicates that Ca was more available than other divalent metals and could satisfy the constant EDTA demand. All these results suggest that EDTA was in equilibrium with a Ca-supplying phase, which is likely calcite since this mineral is the second most abundant mineral species after quartz according to XRD data. The total amount of Ca solubilized by EDTA after five extraction cycles corresponds to an equivalent concentration of calcite of 12–14 mg/g.

$[Fe]_{aq}$ was relatively constant from one cycle to another, indicating that Fe, similarly to Ca, was available on EDTA demand, i.e. in equilibrium with an Fe solid phase. More precisely, $[Fe]_{aq}$ decreased slightly from 2.48 to 2.31 mmol/L between the 1st and 2nd cycle (Table 4). From the 4th to the 5th cycle, $[Fe]_{aq}$ increased significantly by 0.06 mmol/L (from 0.235 to 0.293 mmol/L), whereas $[Ca]_{aq}$ concomitantly decreased by 0.7 mmol/L (from 6.41 to 5.71 mmol/L). This finding suggests that Ca became less available than Fe in the 5th cycle, and that the amount of the Fe-EDTA complex in solution increased relative to that of the Ca–EDTA.

Since $[Ca]_{aq}$ and $[Fe]_{aq}$ as well as the Ca- and Fe-supplying solids are in equilibrium with EDTA, $[Ca]_{aq}$ and $[Fe]_{aq}$ can be predicted from equilibrium speciation calculation. This calculation was performed with the Phreeqc for Windows code (Parkhurst and Appelo, 1999) using the Phreeqc formatted V8.R6 Lawrence Livermore National Laboratory (LLNL) database (Wolery, 1992), unless otherwise noted. Metal–EDTA complexation constants were taken from Smith and Martell (1976) and from the more recent NIST database (Martell and Smith, 2004). The Phreeqc script is presented in *electronic access* EA. From this calculation, a 7 mmol/L Na_2H_2EDTA solution in the presence of excess calcite and ferrihydrite equilibrates theoretically at pH 7.0 and at a molar ratio $MR_{Ca} = [Ca]_{aq}/([Ca]_{aq} + [Fe]_{aq}) = 80\%$. When forcing the system to the experimental pH value measured in the 1st cycle (pH 7.5), calculated MR_{Ca} equals 95.5%, which matches the experimental MR_{Ca} values for all cycles (95.0–96.5%, Table 4). Thus, our equilibrium model and data both predict a Ca over Fe dominance in solution for all extraction cycles. Note that the MR_{Ca} parameter is a good indicator of the equilibrium state of the system, because its value is essentially independent of the presence or absence of other dissolved MVCs. Also, and consistently with the assumed equilibrium condition, speciation calculations showed that 99.999% of EDTA was complexed to MVCs and, conversely, that most of the MVCs were complexed to EDTA.

The ferrihydrite solubility constant which yielded the best agreement between experiment and theory was that given by Dzombak and Morel (1990) for hydrous ferric oxide

$$Fe(OH)_3 + 3H^+ \leftrightarrow Fe^{3+} + 3H_2O; \quad \log K_{s-Fe}=2.5 \qquad (2)$$

The solubility constant given for aged $FeOH_{3(s)}$ in the NIST database ($\log K_{s-Fe} = 2.69$; Martell and Smith, 2004) compares closely. Using the NIST value for non-aged $FeOH_{3(s)}$ ($\log K_{s-Fe} = 3.39$) decreased MR_{Ca} to 75%, consistently with the lower solubility of aged vs. non-aged ferrihydrite. Using the solubility constants given for ferrihydrite in the Minteq database ($\log K_{s-Fe} = 4.89$; Jerry et al., 1991) and in the Phreeqc built-in LLNL V8.R6 database ($\log K_{s-Fe} = 5.66$, Wolery, 1992) decreased MR_{Ca} to 31 and 25%, respectively, thus predicting an Fe over Ca dominance, in contrast to the data. None of the solubility constants available for well crystalline Fe oxides described the data. For example, using the solubility constant for goethite ($\log K_{s-Fe} = 0.491$, NIST database) resulted in $MR_{Ca} = 99.9\%$ after the first extraction, that is predicting a $[Fe]_{aq}$ value of 3.5 μmol/L instead of 248 μmol/L. Similar, or even lower $[Fe]_{aq}$ values, were obtained with other well crystalline Fe oxides, indicating that the Fe availability in the cycling EDTA extraction experiments was not controlled by crystallized Fe oxide. The ferrihydrite dissolved during the first extraction cycle did not release Zn since the proportion of the Zn-ferrihydrite species, as determined by EXAFS spectroscopy, remained essentially the same before and after chemical treatment. Thus, Zn ferrihydrite seems less soluble than ferrihydrite that does not bear Zn. Since the studied soil has been irrigated by sewage water for 100 years, Zn may be occluded in fine-grained crystalline aged ferrihydrite.

Aqueous concentrations of Cu, Zn, Pb, and P decreased with the increasing number of cycles. This result suggests that these metals are co-associated with phosphate, in agreement with EXAFS and SXRF results. This hypothesis was tested by calculating the aqueous concentration of Zn-EDTA at pH 7.5 and 7 mmol/L EDTA in a quaternary system comprising calcite, ferrihydrite, gibbsite and one of the following phosphate minerals: hopeite ($Zn_3(PO_4)_2 \cdot 4H_2O$), scholzite ($Zn_2Ca(PO_4)_2 \cdot (H_2O)_2$), spencerite ($Zn_4(PO_4)_2(OH)_2$), Zn–pyromorphite ($Zn_5(PO_4)_3Cl$), or tarbuttite ($Zn_2(PO_4)OH$). We used the same solubility constants as Panfili et al. (2005) for the Zn phosphate compounds. The percentage of EDTA complexed to Zn in the five systems was as high as 98.8, 99.7, 99.5, 98.7, and 76%, respectively. This means that EDTA has a much stronger affinity for Zn than for the other major MVCs in equilibrium with the solid phases of the mixture (i.e., Ca, Fe, Al). Also, in all explored systems calculated $[Zn]_{aq}$ was higher than the total Zn content in the soil (17 μmol/g in the soil, i.e., 3.4 mmol/L in the 200 g/L suspension), which means that when in equilibrium with calcite, ferrihydrite and gibbsite, EDTA can theoretically dissolve all tested Zn phosphate minerals. Thus, our thermodynamic calculations support the quantitative solubilization of the Zn–phosphate species revealed by EXAFS spectroscopy. Zn kerolite was the only tested Zn phase that was thermodynamically stable under our experimental conditions. This result is consistent with EXAFS results, since this phase was shown to be essentially inert to EDTA.

4.2.2. EDDS

Although the same extraction conditions were applied for EDTA and EDDS, i.e., 7 mmol/L chelant concentration and 200 g/L solid content, marked differences were observed in the major element composition of the supernatants. In the EDDS experiment, $[Ca]_{aq}$ (2.53–2.93 mmol/L) was typically half that in the EDTA experiment (Table 4), but $[Ca]_{aq}$ remained constant in both cases upon renewing the extracting solution, indicating that Ca was always 'available on demand.' In contrast, $[Fe]_{aq}$ (1.0–1.8 mmol/L) and $[Al]_{aq}$ (0.32–1.25 mmol/L) were higher with EDDS than with EDTA (0.23–0.29 mmol/L, and 21–39 μmol/L, respectively). Another difference is the decrease of the amount of Fe and Al solubilized with EDDS upon renewing the chelant, which is an indication of the progressive exhaustion of the Fe and Al supplies. Few differences were observed with heavy metals, although slightly more were extracted with EDDS than with EDTA: $[Zn]_{aq}$ ranged from 0.12 to 1.43 mmol/L with EDDS and from 0.10 to 2.27 mmol/L with EDTA, $[Cu]_{aq}$ from 0.029 to 0.67 mmol/L with EDDS and from 0.031 to 0.46 mmol/L with EDTA, and $[Pb]_{aq}$ from 0.032 to 0.17 mmol/L with EDDS and from 0.021 to 0.13 mmol/L with EDTA. Also, the metal concentrations always decreased with the number of cycles. Consequently, metal extraction data may not be interpreted in terms of metal–ligand complexation strength (or metal selectivity) under equilibrium conditions.

Phreeqc simulations were performed with 7 mmol/L EDDS at pH 7.5 (the experimental value) assuming, first, an excess of calcite, ferrihydrite and gibbsite only. Calculated $[Ca]_{aq}$ (2.5 mmol/L) compared well with measured $[Ca]_{aq}$ (2.5–2.9 mmol/L), with the majority of calculated $[Ca]_{aq}$ being uncomplexed (2.2 mmol/L). Similarly to Ca, our calculation predicted that most of the EDDS (89%) remained uncomplexed in solution, in contrast to the EDTA experiment. Thus, EDDS appears to be a much weaker Ca complexant than EDTA, consistent with the six orders of magnitude difference between the Ca–EDDS and Ca–EDTA complexation constants (Martell and Smith, 2004). In strong contrast with Ca, but also in agreement with log K values, EDDS was found to bind metals strongly, in particular Zn, as 99.99 and 94% of EDDS was complexed to Zn and Pb, respectively, when hopeite (Zn) and cerussite (Pb) were added in excess to the three previous solids. Therefore, EDDS and EDTA have mostly comparable extraction capabilities for heavy metals, but not for calcium. This difference of binding properties between EDDS and EDTA may explain why metal extraction levels were significantly higher with the first complexant since part of the EDTA in contact with the soil may have been complexed by Ca, whose content is relatively high ([CaO] = 3.4%) (Fig. 1).

In field conditions, EDTA and EDDS will be less concentrated than in our experimental setup. To test their relative efficiency toward metal extraction in dilute systems, and more especially toward Zn from hopeite, another simulation was performed for the same quaternary system at 10^{-5} mol/L ligand concentration. At this concentration, EDTA and EDDS still are excellent metal extractants from solid phases since 99.99% of EDDS and 99.95% of EDTA were complexed to Zn. In the same conditions, only 1.7% of citrate was complexed to Zn. However, it will be seen below that citrate, in combination with soil microorganisms, may dissolve reducible phases, such as Fe oxyhydroxides, thereby releasing associated trace metals. Therefore, the relative affinity of EDDS and EDTA, on one hand, and of citrate, on the other hand, also depends on the nature of the host phase, and there may be cases in which citrate is a better extractant than the other two chelants.

Two indirect lines of evidence support the hypothesis that EDDS may be a reductant under certain conditions, although to a lesser extent than citrate. The first comes from the difference between the measured (1.0–1.8 mmol/L) and the calculated (0.4 mmol/L) concentrations of Fe in the ternary model system. Second is the fact that EDDS always extracted more metals than EDTA, as apparent in Fig. 1. These two observations suggest that EDDS is a weak Fe(III) reducing reagent. If our hypothesis is valid, then EDDS can extract trace metals by two complementary mechanisms: complexation of metals contained in non-reducible host phases, and reductive dissolution of metal-containing host phases. Since EDDS is rapidly degraded in soils (Vandevivere et al., 2001b), one may infer that its (bio)degradation may be coupled with Fe reduction.

4.2.3. Citrate

Equilibrium calculations showed that citrate is a weaker ligand than EDTA and EDDS, and does not preferentially extract heavy metals from the solid phases. Under equilibrium conditions at pH 7.8 (i.e., the experimental value of the 1st citrate cycle), none of the tested solid phases (calcite, ferrihydrite, gibbsite, metal phosphate) was completely dissolved when reacted separately with 0.1 mol/L citrate and assuming an MVC concentration of 0.05 mol/L in the solid; i.e., a 100% excess of citrate. The same calculation, but with the presence of an excess of calcite, ferrihydrite and gibbsite (i.e., ternary system) yielded $[Ca]_{aq} = 21$ mmol/L, $[Fe]_{aq} = 0.11$ μmol/L, and $[Al]_{aq} = 11$ mmol/L. As much as 43% of the initial citrate remained free. The effect of citrate on a particular MVC-containing phase can be predicted by simulating a system in which only the MVC-supplying phase is in excess. For example, a 0.1 mol/L suspension of citrate at pH 7.8 containing only hopeite as the solid phase yielded $[Zn]_{aq}$ (or Zn–citrate) = 2.5 mmol/L, meaning that only 2.5% of citrate was complexed to Zn. Adding an excess of calcite, gibbsite and ferrihydrite to this suspension reduced the free ligand concentration from 97.5 to 41%, and also decreased $[Zn]_{aq}$ from 2.5 to 1.3 mmol/L. The same general effect was observed with other Zn-containing phases. These calculations show that citrate does not dissolve selectively metal-containing phases. More generally, our calculations showed that at equilibrium with a mixture of solid phases, citrate

prefers calcite and ferrihydrite to the metalliferous phases. The lack of citrate selectivity for metal-containing phases contrasts with EDTA and EDDS. However, in the conditions of our experiments the dissolution of metal phases may have been complete since citrate was in large excess relative to the total amount of Cu, Zn, and Pb.

In the cycling citrate extraction experiment, Ca was, in agreement with equilibrium calculations, the most extracted MVC (Table 4). In the 1st cycle, $[Ca]_{aq} = 13.7$ mmol/L, a value slightly lower than the theoretical value (21 mmol/L) at pH 7.8 (i.e., fixed to the experimental value) and in the presence of an excess of calcite, ferrihydrite and gibbsite. The solubility of Ca continuously decreased afterwards from the 2nd to 5th cycle. After the 1st cycle, $[Ca]_{aq}$ corresponded to an extracted Ca amount of 172 μmol Ca/g soil, which is more than the total amount of Ca extracted in all the five EDTA (144 μmol Ca/g soil) and EDDS (67 μmol Ca/g soil) cycles. The higher amount of extracted Ca is mainly due to the higher amount of citrate used here compared to the EDTA and EDDS experiments (Table 1).

Fe was the second highest MVC extracted by citrate (Table 4). $[Fe]_{aq}$ increased slightly from the 1st (2.27 mmol/L) to the 2nd (2.57 mmol/L) cycle, due probably to an increase of free citrate concentration in the 2nd cycle as a result of the concomitant decrease of Ca–citrate. Afterwards, $[Fe]_{aq}$ decreased from 2.57 (2nd) to 0.287 (5th) mmol/L, indicating that the Fe availability decreased. The declining availability of these elements suggests that only the most easily dissolved phases (e.g., fine-grained and amorphous phases) are removed. Experimental $[Fe]_{aq}$ values measured in the 1st and 2nd cycles were inconsistent with the predicted value from equilibrium calculations (0.05 μmol/L). Substitution of the solubility constant for Fe oxide that best-fitted the EDTA data ($\log K_{s\text{-}Fe} = 2.5$) by the solubility constant from the Minteq database ($\log K_{s\text{-}Fe} = 4.9$) raised the calculated $[Fe]_{aq}$ to 20 μmol/L but, still, did not account for the experimental concentration. In fact, the predicted and experimental values are so different that a solubilization mechanism other than Fe(III)-ligand equilibrium complexation must have occurred, such as reduction of Fe(III) to Fe(II).

In the presence of a reducing agent, such as dithionite, poorly and well crystallized iron oxides are efficiently and selectively dissolved by citrate, whose role is to complex Fe(II) and to prevent its readsorption on reactive mineral surfaces (Kostka and Luther, 1994; Soulier et al., 1994; Trolard et al., 1995). Since our dissolution experiments were performed in a closed reactor, anoxic conditions may have been created by the metabolic activity of some common O_2-scavenging bacteria, such as *Escherichia coli*, *Lactococcus lactis* or *Pseudomonas stutzer* (Straub and Schink, 2004).

Experimental $[Al]_{aq}$ measured at the end of the 1st citrate cycle (0.85 mmol/L) is slightly below the calculated equilibrium concentration (2.8 mmol/L) for the calcite–ferrihydrite–gibbsite ternary system. Given that $[Al]_{aq}$ decreased in the following cycles along with other MVCs, this result suggests that the Al-supplying solid is soluble in citrate.

Of the heavy metals extracted by citrate, Zn is the most prevalent (Table 4). As for EDTA, Zn and P followed the same solubilization pattern with repeated citrate extraction. The parallel dissolution of Zn and P is consistent with the EXAFS results, which showed that the Zn phosphate component was quantitatively dissolved after the 1st citrate extraction cycle. The $[Zn]_{aq}/[P]_{aq}$ ratio after the 1st cycle (0.4) is lower than the stoichiometric Zn/P ratio of our Zn phosphate dihydrate model compound. This discrepancy can be explained by the fact that citrate lacks selectivity for heavy metals relative to background cations (Table 2). To verify this interpretation, equilibrium speciation calculations were performed for a model citrate solution containing an excess of calcite, ferrihydrite, gibbsite, and Zn speciated as hopeite. The calculated Zn solubility was 1.38 mmol/L, that is 239, 100, and 93% of the amount measured after the 1st extraction cycle with citrate (0.59 mmol/L), EDTA (1.36 mmol/L), and EDDS (1.43 mmol/L). These results confirm that in a phase mixture citrate does not dissolve preferentially the metal-containing phases, in contrast to EDTA and EDDS. In our experiment, the Zn phosphate component was dissolved quantitatively during the 1st cycle because citrate was added in excess relative to the metal and background Fe and Ca cations in the soil (Table 1). More generally, results from Fig. 1 may give the false impression that citrate is as efficient as EDTA and EDDS in extracting metals. In fact, the similar extractability of metals with the three ligands is due to the fact that the chemical reactors contained 14 times more citrate than EDTA and EDDS (i.e., 100 vs. 7 mmol/L), and a solid to solution ratio 2.5 times lower than that in the citrate reactor (80 vs. 200 g/L). Therefore, the lower affinity of citrate for metals was compensated by increasing its concentration and decreasing the amount of solid in the reactor.

4.3. Environmental implications

The extraction levels measured in the desorption experiments indicated that significant removal of heavy metals could be obtained on a time scale of hours. Therefore, adding chelating agents to the Pierrelaye soil is a possible remediation approach. The use of EDDS and citrate, and especially of citrate whose cost is relatively low, is attractive because these molecules and their metal complexes are easily biodegraded and, therefore, do not have long-lasting effects (Dodge and Francis, 1994; Huang et al., 1998; Vandevivere et al., 2001b). Citrate rapidly dissociates to carbon dioxide and water, thus preventing the dispersion of its metal complexes into surface and ground waters. However, the biodegradability of metal–citrate complexes highly depends on their nature. For example, the tridentate complexes of citrate with Cu and Pb are more resistant to bacterial degradation than the bidentate complexes with Fe and Ni (Francis et al., 1992). Note that the longer life-time of some complexes may be an advantage in the treatment

of certain locations such as wastewater plants, because it may allow the recovery of the metal. Finally, both EDDS and citrate are classified as non-hazardous chemicals to humans and the environment.

In contrast, and despite its high mobilizing capacity and selectivity for heavy metals, EDTA is not suitable for remediation because of its slow biodegradability (Bolton et al., 1993; Regmi et al., 1996; Egli, 2001). It has been reported that EDTA and its complexes can persist in the environment over several years, with heavy metal–EDTA complexes, including Zn, Cu, and Pb, being the most persistent (Nowack et al., 1997; Satroutdinov et al., 2000). Also, conventional biological and chemical wastewater treatments are not efficient for degrading EDTA-containing effluents (Gardiner, 1976; Hinck et al., 1997). In addition to being weakly biodegraded, EDTA has been reported to be toxic to photosynthetic organisms, inhibiting cellular division, chlorophyll synthesis and algal biomass production (Dufková, 1984). In an experiment on living rat kidney cells, Hugenschmidt et al. (1993) showed that at concentrations of Na_2H_2EDTA lower than 100 μM, which was less than the concentration required to chelate all of the free Ca^{2+} ions in the growth medium, many cells died, and cell division was severely impaired.

5. Concluding remarks

This study documents the usefulness of combining state-of-the-art X-ray techniques, modern EXAFS data reduction (i.e., PCA and LCF), chemical extractions, and thermodynamic modeling to identify and quantify the solid state forms of metals in contaminated soil, and to evaluate the modification of metal speciation upon adding organic ligands. Zinc is predominantly, and almost evenly, bound to iron oxyhydroxide (~30%), phosphate (~28%), and phyllosilicate (~24%) in the studied near-neutral (pH 6.5–7.0) truck farming soil contaminated by sewage irrigation. Thus, these three secondary phases control the mobility and, in particular the bioavailability, of zinc in the field. As much as ~40% of the soil Zn was solubilized with citrate, EDDS, and EDTA in a few hours of reaction time, and up to ~80% with citrate when the extracting solution was renewed. Therefore, citrate, which is relatively cheap and easily biodegraded, may be used to remediate this soil. EXAFS revealed that the three chelants dissolved Zn phosphate selectively in the laboratory after 24 h of contact time. The other coexisting zinc species were either not or else only moderately affected by a single extraction step, but more solubilized when the chelating solution is renewed. This study also shows that there is no direct correlation between the amount of metal extracted and the metal–ligand thermodynamical binding constant.

Acknowledgments

The authors are grateful to Jean-Louis Hazemann, Olivier Proux, and Jean-Jacques Menthonnex for their assistance during EXAFS measurements on the FAME beamline at ESRF, and to Sébastien Pairis for his assistance in collecting SEM-EDS data. Géraldine Sarret is acknowledged for insightful discussions, and two anonymous reviewers and Dr. A.C. Scheinost for their constructive remarks. We also thank Martine Lanson and Nicolas Geoffroy for their analytical and technical assistance. EDDS was kindly provided by Sigma–Aldrich Fluka. The CNRS, which supports the French-CRG program at ESRF, and the ALS are acknowledged for the provision of beamtime. Finally, we thank *Phytorestore* and ANRT for fellowship support of T.A.K. during this study, and also the Region Ile-de-France for partial support of this research.

Associate editor: Garrison Sposito

Appendix A. Supplementary data

Supplementary data associated with this article can be found, in the online version, at doi:10.1016/j.gca.2006.02.006.

References

Acar, Y.B., Gale, R.J., 1995. Electrokinetic remediation: basic and technology status. *J. Hazard. Mater.* **40**, 117–137.

Anderson, C.W.N., Brooks, R.R., Stewart, R.B., Simcock, R., 1998. Harvesting a crop of gold in plants. *Nature* **395**, 553–554.

Baize, D., 2000. Teneurs en métaux lourds dans les sols français. *Courrier de l'environnement de l'INRA* **22**, 39–54.

Baize, D., Lamy, I., Van Oort, F., Dere, C., Chaussod, R., Sappin-Didier, V., Bermond, A., Bourgeous, S., Schmitt, C., Schwartz, C., 2002. 100 years spreading of urban waste water on market-garden soils close to Paris (France): subsequent impacts and hazards. In: *17th World Congress of Soil Science*, Bangkok, Thailand, pp. 1–10.

Bassi, R., Prasher, S.O., Simpson, B.K., 2000. Extraction of metals from a contaminated sandy soil using citric acid. *Environ. Prog.* **19**, 275–282.

Blais, J.F., Tyagy, R.D., Auclair, J.C., 1992. Bioleaching of metals from sewage sludge by sulfur-oxidizing bacteria. *J. Environ. Eng. ASCE* **118**, 690–707.

Blaylock, M.J., Salt, D.E., Dushenkov, S., Zakharova, O., Gussman, C., Kapulnik, Y., Ensley, B.D., Raskin, Y., 1997. Enhanced accumulation of Pb in Indian Mustard by soil-applied chelating agents. *Environ. Sci. Technol.* **31**, 860–865.

Blaylock, M.J., 2000. Field demonstration of phytoremediation of lead contaminated soils. In: *Phytoremediation of Contaminated Soil and Water*. Lewis Publ., Boca Raton, FL, pp. 1–12.

Bolton Jr., H., Li, S.W., Workman, D.J., Girvin, D.C., 1993. Biodegradation of synthetic chelates in subsurface sediments from the southeast coastal plain. *J. Environ. Qual.* **22**, 125–132.

Buatier, M.D., Sobanska, S., Elsass, F., 2001. TEM-EDX investigation on Zn- and Pb-contaminated soils. *Appl. Geoch.* **16**, 1165–1177.

Calmano, W., Mangold, S., Welter, E., 2001. An XAFS investigation of the artefacts caused by sequential extraction analyses of Pb-contaminated soils. *Fres. J. Anal. Chem.* **371**, 823–830.

Cline, S.R., Reed, B.R., 1995. Lead removal from soils via bench-scale soil washing techniques. *J. Environ. Eng. ASCE* **121**, 700–705.

Cooper, E.M., Sims, J.T., Cunningham, S.D., Huang, J.W., Berti, W.R., 1999. Chelate-assisted phytoextraction of lead from contaminated soils. *J. Environ. Qual.* **28**, 1709–1719.

Cornell, R.M., 1988. The influence of some divalent cations on the transformation of ferrihydrite to more crystalline products. *Clay Minerals* **23**, 329–332.

Cornell, R.M., Schwertmann, U., 1996. *The Irons Oxides: Structure, Properties, Reactions, Occurrence and Uses*. VCH Publishers, New York.

Cotter-Howells, J., Caporn, S., 1996. Remediation of contaminated land by formation of heavy metal phosphates. *Appl. Geochem.* **11**, 335–342.

Cotter-Howells, J.D., Champness, P.E., Charnock, J.M., 1999. Mineralogy of lead–phosphorus grains in the roots of Agrostis capillaris L. by ATEM and EXAFS. *Mineral Mag.* **63**, 777–789.

Cotter-Howells, J.D., Champness, P.E., Charnock, J.M., Pattrick, R.A.D., 1994. Identification of pyromorphite in mine-waste contaminated soils by ATEM and EXAFS. *Eur. J. Soil Sci.* **45**, 393–402.

Cunningham, S.D., Berti, W.R., 1993. Remediation of contaminated soils with green plants: An overview. *In Vitro Cell. Dev. B* **29**, 207–212.

Davis, J.A., Kent, D.B., 1990. Surface complexation modeling in aqueous geochemistry. In: Hochella, M.F., White, A. (Eds.), *Reviews in Mineralogy and Geochemistry, vol. 23: Mineral–Water Interface Geochemistry*. Mineralogical Society of America, Washington, DC, pp. 177–260.

Dodge, C.J., Francis, A.J., 1994. Photodegradation of uranium–citrate complex with uranium recovery. *Environ. Sci. Technol.* **31**, 3062–3067.

Dufková, V., 1984. EDTA in algal culture media. *Arch. Hydrobiol. Suppl.* **67**, 479–492.

Dzombak, D.A., Morel, M.M.F., 1990. *Surface Complexation Modelling*. John Wiley & Sons, New York.

Ebbs, S.D., Lasat, M.M., Brady, D.J., Cornish, J., Gordon, R., Kochian, L.V., 1997. Phytoextraction of cadmium and zinc from a contaminated soil. *J. Environ. Qual.* **26**, 1424–1430.

Ebbs, S.D., Kochian, L.V., 1998. Phytoextraction of zinc by oat (*Avena sativa*), barley (*Hordeum vulgare*), and Indian mustard (*Brassica juncea*). *Environ. Sci. Technol.* **32**, 802–806.

Ebbs, S.D., Norvell, W.A., Kochian, L.V., 1998. The effect of acidification and chelating agents on the solubilization of uranium from contaminated soil. *J. Environ. Qual.* **27**, 1486–1494.

Egli, T., 2001. Biodegradation of metal-complexing aminopolycarboxylic acids. *J. Biosci. Bioeng.* **92**, 89–97.

Elliott, H.A., Brown, G.A., 1989. Comparative evaluation of NTA and EDTA for extractive decontamination of Pb-polluted soils. *Water, Air, Soil Pollut.* **45**, 361–369.

Foster, A.L., Brown, G.E., Tingle, T.N., Parks, G.A., 1998. Quantitative arsenic speciation in mine tailings using X-ray absorption spectroscopy. *Am. Miner.* **83**, 553–568.

Francis, A.J., Dodge, C.J., Gillow, J.B., 1992. Biodegradation of metal citrate complexes and implications for toxic-metal mobility. *Nature* **356**, 140–142.

Gaillard, J.F., Webb, S.M., Quintana, J.P.G., 2001. Quick X-ray absorption spectroscopy for determining metal speciation in environmental samples. *J. Synchrotron Rad.* **8**, 928–930.

Gardiner, J., 1976. Complexation of trace metals by ethylendiaminetetraacetic acid (EDTA) in natural waters. *Water Res.* **10**, 507–514.

Ghestem, J.P., Bermond, A., 1998. EDTA extractability of trace metals in polluted soils: A chemical–physical study. *Environ. Technol.* **19**, 409–416.

Grcman, H., Vodnik, D., Velikonja Bolta, S., Lestan, D., 2003. Ethylenediaminedissuccinate as a new chelate for environmentally safe enhanced: Lead phytoextraction. *J. Environ. Qual.* **32**, 500–506.

Gruebel, K.A., Davis, J.A., Leckie, J.O., 1988. The feasibility of using sequential extraction techniques for arsenic and selenium in soils and sediments. *Soil Sci. Soc. Am. J.* **52**, 390–397.

Hansel, C.M., Fendorf, S., Sutton, S., Newville, M., 2001. Characterization of Fe plaque and associated metals on the roots of mine-waste impacted aquatic plants. *Environ. Sci. Technol.* **35**, 3863–3868.

Hettiarachchi, G.M., Pierzynski, G.M., Ransom, M.D., 2000. In situ stabilization of soil lead using phosphorus and manganese oxide. *Environ. Sci. Technol.* **34**, 4614–4619.

Hinck, M.L., Ferguson, J.F., Puhakka, J.A., 1997. Resistance of EDTA and DTPA to aerobic biodegradation. *Water Sci. Technol.* **35**, 25–31.

Hinsinger, P., 2001. Bioavailability of trace elements as related to root-induced chemical changes in the rhizosphere. In: Gobran, G.R., Wenzel, W.W., Lombi, E. (Eds.), *Trace Elements in the Rhizosphere*. CRC Press LCC, Boca Raton, Florida, USA, pp. 25–41.

Hochella, M.F., Moore, J.N., Golla, U., Putnis, A., 1999. A TEM study of samples from acid mine drainage systems: Metal–mineral association with implications for transport. *Geochim. Cosmochim. Acta* **63**, 3395–3406.

Huang, J.W., Chen, J., Berti, W.R., Cunningham, S.D., 1997. Phytoremediation of lead-contaminated soils: Role of synthetic chelates in lead phytoextraction. *Environ. Sci. Technol.* **31**, 800–805.

Huang, J.W.W., Blaylock, M.J., Kapulnik, Y., Ensley, B.D., 1998. Phytoremediation of uranium contaminated soils: Role of organic acids in triggering uranium hyperaccumulation in plants. *Environ. Sci. Technol.* **32**, 2004–2008.

Hugenschmidt, S., Planas-Bohne, F., Taylor, D., 1993. On the toxicity of low doses of tetrasodium–ethylenediaminetetraacetate (Na–EDTA) in normal rat kidney (NRK) cells in culture. *Arch. Toxicol.* **67**, 76–78.

Isaure, M.P., Laboudigue, A., Manceau, A., Sarret, G., Tiffreau, C., Trocellier, P., Lamble, G., Hazemann, J.L., Chateigner, D., 2002. Quantitative Zn speciation in a contaminated dredged sediment by μ-PIXE, μ-SXRF, EXAFS spectroscopy and principal component analysis. *Geochim. Cosmochim. Acta* **66**, 1549–1567.

Isaure, M.P., Manceau, A., Geoffroy, N., Laboudigue, A., Tamura, N., Marcus, M.A., 2005. Zinc mobility and speciation in soil covered by contaminated dredged sediment using micrometer-scale and bulk-averaging X-ray fluorescence, absorption and diffraction techniques. *Geochim. Cosmochim. Acta* **69**, 1173–1198.

Jerry, D.A., Brown, D.S., Novo-Gradac, K.J., 1991. *MINTEQA2/PRODEFA2, a geochemical assesment model for environmental systems: User's manual, version 3.0, US EPA/600/3-91/021 Report*.

Juillot, F., Morin, G., Ildefonse, P., Trainor, T.P., Benedetti, M., Galoisy, L., Calas, G., Brown, G.E., 2003. Occurrence of Zn/Al hydrotalcite in smelter-impacted soils from northern France: Evidence from EXAFS spectroscopy and chemical extractions. *Am. Miner.* **88**, 509–526.

Kayser, A., Wenger, K., Keller, A., Attinger, W., Felix, H.R., Gupta, S.K., Schulin, R., 2000. Enhancement of phytoextraction of Zn, Cd, and Cu from calcareous soil: The use of NTA and sulfur amendments. *Environ. Sci. Technol.* **34**, 1778–1783.

Kim, C.S., Bloom, N.S., Rytuba, J.J., Brown, G.E., 2003. Mercury speciation by X-ray absorption fine structure spectroscopy and sequential chemical extractions: A comparison of speciation methods. *Environ. Sci. Technol.* **37**, 5102–5108.

Kneebone, P.E., O'Day, P.A., Jones, N., Hering, J.G., 2002. Deposition and fate of arsenic in iron- and arsenic-enriched reservoir sediments. *Environ. Sci. Technol.* **36**, 381–386.

Kostka, J.E., Luther, G.W., 1994. Partitioning and speciation of solid phase iron in saltmarsh sediments. *Geochim. Cosmochim. Acta* **58**, 1701–1710.

La Force, M.J., Fendorf, S., 2000. Solid-phase iron characterization during common selective sequential extractions. *Soil Sci. Soc. Am. J.* **64**, 1608–1615.

Linn, J.H., Elliott, H.A., 1988. Mobilisation of Cu and Zn in contaminated soil by NTA. *Water, Air, Soil Pollut.* **37**, 449–458.

Lombi, E., Zhao, F.J., Dunham, S.J., McGrath, S.P., 2001. Phytoremediation of heavy metal-contaminated soils: Natural hyperaccumulation versus chemically enhanced phytoextraction. *J. Environ. Qual.* **30**, 1919–1926.

Malinowski, E.R., 1991. *Factor Analysis in Chemistry*. John Wiley, New York.

Manceau, A., Llorca, S., Calas, G., 1987. Crystal chemistry of cobalt and nickel in lithiophorite and asbolane from New Caledonia. *Geochim. Cosmochim. Acta* **51**, 105–113.

Manceau, A., Boisset, M.C., Sarret, G., Hazemann, J.L., Mench, M., Cambier, P., Prost, R., 1996. Direct determination of lead speciation in contaminated soils by EXAFS spectroscopy. *Environ. Sci. Technol.* **30**, 1540–1552.

Manceau, A., Chateigner, D., Gates, W.P., 1998. Polarized EXAFS, distance-valence least-squares modeling (DVLS) and quantitative texture analysis approaches to the structural refinement of Garfield nontronite. *Phys. Chem. Mineral* **25**, 347–365.

Manceau, A., Schlegel, M., Nagy, K.L., Charlet, L., 1999. Evidence for the formation of trioctahedral clay upon sorption of Co^{2+} on quartz. *J. Colloid Interf. Sci.* **220**, 181–197.

Manceau, A., Lanson, B., Schlegel, M.L., Harge, J.C., Musso, M., Eybert Berard, L., Hazemann, J.L., Chateigner, D., Lamble, G.M., 2000a. Quantitative Zn speciation in smelter-contaminated soils by EXAFS spectroscopy. *Am. J. Sci.* **300**, 289–343.

Manceau, A., Schlegel, M.L., Musso, M., Sole, V.A., Gauthier, C., Petit, P.E., Trolard, F., 2000b. Crystal chemistry of trace elements in natural and synthetic goethite. *Geochim. Cosmochim. Acta* **64**, 3643–3661.

Manceau, A., Tamura, N., Marcus, M.A., MacDowell, A.A., Celestre, R.S., Sublett, R.E., Sposito, G., Padmore, H.A., 2002a. Deciphering Ni sequestration in soil ferromanganese nodules by combining X-ray fluorescence, absorption and diffraction at micrometer scales of resolution. *Am. Miner.* **87**, 1494–1499.

Manceau, A., Marcus, M.A., Tamura, N., 2002b. Quantitative speciation of heavy metals in soils and sediments by synchrotron X-ray techniques. In: Fenter, P., Rivers, M., Sturchio, N.C., Sutton, S. (Eds.), *Reviews in Mineralogy and Geochemistry, vol. 49: Applications of Synchrotron Radiation in Low-Temperature Geochemistry and Environmental Science*. Mineralogical Society of America, Washington, DC, pp. 341–428.

Manceau, A., Tamura, N., Celestre, R.S., MacDowell, A.A., Geoffroy, N., Sposito, G., Padmore, H.A., 2003a. Molecular-scale speciation of Zn and Ni in soil ferromanganese nodules from loess soils of the Mississippi basin. *Environ. Sci. Technol.* **37**, 75–80.

Manceau, A., Lanson, B., Drits, V.A., 2003b. Structure of heavy metal sorbed birnessite. Part III: Results from powder and polarized EXAFS spectroscopy. *Geochim. Cosmochim. Acta* **66**, 2639–2663.

Manceau, A., Marcus, M.A., Tamura, N., Proux, O., Geoffroy, N., Lanson, B., 2004. Natural speciation of Zn at the micrometer scale in a clayey soil using X-ray fluorescence, absorption, and diffraction. *Geochim. Cosmochim. Acta* **68**, 2467–2483.

Manceau, A., Tommaseo, C., Rihs, S., Geoffroy, N., Chateigner, D., Schlegel, M., Tisserand, D., Marcus, M.A., Tamura, N., Chen, Z.S., 2005. Natural speciation of Mn, Ni and Zn at the micrometer scale in a clayey paddy soil using X-ray fluorescence, absorption, and diffraction. *Geochim. Cosmochim. Acta* **69**, 4007–4034.

Marcus, M.A., MacDowell, A.A., Celestre, R., Manceau, A., Miller, T., Padmore, H.A., Sublett, R.E., 2004. Beamline 10.3.2 at ALS: a hard X-ray microprobe for environmental and materials sciences. *J. Synchrotron Rad.* **11**, 239–247.

Martell, A.E., Smith, R.M., Motekaitis, R.J., 2001. *NIST Critically Selected Stability Constants of Metal Complexes, Version 6*. NIST, Gaithersburg, MD, USA.

Martell, A.E., Smith, R.M., 2004. *NIST Critically Selected Stability Constants of Metal Complexes, Version 8.0*. NIST, Gaithensburg, MD, USA.

McGrath, S.P., 1998. Phytoextraction for soil remediation. In: Brooks, R.R. (Ed.), *Plants That Hyperaccumulate Heavy Metals. Their Role in Phytoremediation, Microbiology, Archaeology, Mineral Exploration and Phytomining*. CAB International, Wallingford, UK, pp. 261–287.

Morin, G., Ostergren, J.D., Juillot, F., Ildefonse, P., Calas, G., Brown, G.E., 1999. XAFS determination of the chemical form of lead in smelter-contaminated soils and mine tailings: Importance of adsorption processes. *Am. Miner.* **84**, 420–434.

Morin, G., Juillot, F., Ildefonse, P., Calas, G., Samama, J.C., Chevallier, P., Brown, G.E., 2001. Mineralogy of lead in a soil developed on a Pb-mineralized sandstone (Largentière, France). *Am. Miner.* **86**, 92–104.

Mulligan, C.N., Yong, R.N., Gibbs, B.F., 2001. Remediation technologies for metal-contaminated soils and groundwater: an evaluation. *Eng. Geol.* **60**, 193–207.

Nachtegaal, N., Marcus, M.A., Sonke, J.E., Vangronsveld, J., Livi, K., van der Lelie, D., Sparks, D.L., 2005. Effects of in situ remediation on the speciation and bioavailability of zinc in a smelter contaminated soil. *Geochim. Cosmochim. Acta* **69**, 4649–4664.

Norvell, W.A., 1984. Comparaison of chelating agents as extractants for metals in diverse soil materials. *Soil Sci. Soc. Am. J.* **48**, 1285–1292.

Nowack, B., Xue, H., Sigg, L., 1997. Influence of natural and anthropogenic ligands on metal transport during infiltration of river water to groundwater. *Environ. Sci. Technol.* **31**, 866–872.

O'Day, P.A., Carroll, S.A., Waychunas, G.A., 1998. Rock-water interactions controlling zinc, cadmium, and lead concentrations in surface waters and sediments, US Tri-State Mining District. 1. Molecular identification using X-ray absorption spectroscopy. *Environ. Sci. Technol.* **32**, 943–955.

O'Day, P.A., Carroll, S.A., Randall, S., Martinelli, R.E., Anderson, S.L., Jelinski, J., Knezovich, J.P., 2000. Metal speciation and bioavailability in contaminated estuary sediments, Alameda Naval Air Station, California. *Environ. Sci. Technol.* **34**, 3665–3673.

Ostergren, J.D., Brown, G.E., Parks, G.A., Tingle, T.N., 1999. Quantitative speciation of lead in selected mine tailings from Leadville, CO. *Environ. Sci. Technol.* **33**, 1627–1636.

Oviedo, C., Rodriguez, J., 2003. EDTA: The chelating agent under environmental scrutiny. *Quim. Nova* **26**, 901–905.

Paktunc, D., Foster, A.L., Laflamme, G., 2003. Speciation and characterization of arsenic in Ketza river mine tailings using X-ray absorption spectroscopy. *Environ. Sci. Technol.* **37**, 2067–2074.

Paktunc, D., Foster, A., Heald, S., Laflamme, G., 2004. Speciation and characterization of arsenic in gold ores and cyanidation tailings using X-ray absorption spectroscopy. *Geochim. Cosmochim. Acta* **68**, 969–983.

Panfili, F., Manceau, A., Sarret, G., Spadini, L., Kirpichtchikova, T., Bert, V., Laboudigue, A., Marcus, M.A., Ahamdach, N., Libert, M.F., 2005. The effect of phytostabilization on Zn speciation in a dredged contaminated sediment using scanning electron microscopy, X-ray fluorescence, EXAFS spectroscopy and principal components analysis. *Geochim. Cosmochim. Acta* **69**, 2265–2284.

Parkhurst, D.L., Appelo, C.A.J., 1999. *User's Guide to PHREEQC (Version 2). A Computer Program for Speciation, Batch-reaction, One-Dimensional Transport, and Inverse Geochemical Calculations. US Geological Survey Water-Resources Investigations Report 99-4259*.

Peters, R.W., 1999. Chelant extraction of heavy metals from contaminated soils. *J. Hazard. Mater.* **66**, 151–210.

Regmi, T., Banerji, S.K., Hong, A., 1996. Biodegradation of chelating agents used for metal removal from contaminated soils. In: *HSRC/WERC Joint Conference on the Environment*, May 21–23, Albuquerque, NM.

Ressler, T., Wong, J., Roos, J., Smith, I., 2000. Quantitative speciation of Mn-bearing particulates emitted from autos burning (methylcyclopentadienyl) manganese tricarbonyl-added gasolines using XANES spectroscopy. *Environ. Sci. Technol.* **34**, 950–958.

Roberts, D.R., Scheinost, A.C., Sparks, D.L., 2002. Zinc speciation in a smelter-contaminated soil profile using bulk and microspectroscopic techniques. *Environ. Sci. Technol.* **36**, 1742–1750.

Robinson, B.H., Brooks, R.R., Clothier, B.E., 1999. Soil amendments affecting nickel and cobalt uptake by *Berkheya coddii*: Potential use for phytomining and phytoremediation. *Ann. Bot.* **84**, 689–694.

Robinson, B.H., Mills, T.M., Petit, D., Fung, L.E., Green, S.R., Clothier, B.E., 2000. Natural and induced cadmium-accumulation in poplar and willow: Implications for phytoremediation. *Plant Soil* **227**, 301–306.

Ryan, J.A., Zhang, P., Hesterberg, D.A., Chou, J., Sayers, D.E., 2001. Formation of chloropyromorphite in lead-contaminated soil amended with hydroxyapatite. *Environ. Sci. Technol.* **35**, 3798–3803.

Salt, D.E., Smith, R.D., Raskin, I., 1998. Phytoremediation. *Ann. Rev. Plant Phys.* **49**, 643–668.

Sarret, G., Manceau, A., Spadini, L., Roux, J.C., Hazemann, J.L., Soldo, Y., EybertBerard, L., Menthonnex, J.J., 1998. Structural determination of Zn and Pb binding sites in *Penicillium chrysogenum* cell walls by EXAFS spectroscopy. *Environ. Sci. Technol.* **32**, 1648–1655.

Sarret, G., Vangronsveld, J., Manceau, A., Musso, M., D'Haen, J., Menthonnex, J.J., Hazemann, J.L., 2001. Accumulation forms of Zn and Pb in *Phaseolus vulgaris* in the presence and absence of EDTA. *Environ. Sci. Technol.* **35**, 2854–2859.

Sarret, G., Saumitou-Laprade, P., Bert, V., Proux, O., Hazemann, J.L., Traverse, A., Marcus, M.A., Manceau, A., 2002. Forms of Zn accumulated in the hyperaccumulator *Arabidopsis halleri. Plant Physiol.* **130**, 1815–1826.

Sarret, G., Balesdent, J., Bouziri, L., Garnier, J.M., Marcus, M.A., Geoffroy, N., Panfili, F., Manceau, A., 2004. Zn speciation in the organic horizon of a contaminated soil by micro-X-ray fluorescence, micro- and powder-EXAFS spectroscopy, and isotopic dilution. *Environ. Sci. Technol.* **38**, 2792–2801.

Satroutdinov, A.D., Dedyukhina, E.G., Chistyakova, T.I., Witschel, M., Minkevich, I.G., Eroshin, V.K., Egli, T., 2000. Degradation of metal–EDTA complexes by resting cells of the bacterial strain DSM 9103. *Environ. Sci. Technol.* **34**, 1715–1720.

Savage, K.S., Tingle, T.N., O'Day, P.A., Waychunas, G.A., Bird, D.K., 2000. Arsenic speciation in pyrite and secondary weathering phases, Mother Lode Gold District, Tuolumne County, California. *Appl. Geochem.* **15**, 1219–1244.

Scheinost, A.C., Kretzschmar, R., Pfister, S., 2002. Combining selective sequential extractions, X-ray absorption spectroscopy, and principal component analysis for quantitative zinc speciation in soil. *Environ. Sci. Technol.* **36**, 5021–5028.

Schlegel, M.L., Manceau, A., Charlet, L., 1997. EXAFS study of Zn and ZnEDTA sorption at the goethite (alpha-FeOOH)/water interface. *J. Phys. IV* **7**, 823–824.

Schlegel, M.L., Manceau, A., Charlet, L., Hazemann, J.L., 2001a. Adsorption mechanisms of Zn on hectorite as a function of time, pH, and ionic strength. *Am. J. Sci.* **301**, 798–830.

Schlegel, M.L., Manceau, A., Charlet, L., Chateigner, D., Hazemann, J.L., 2001b. Sorption of metal ions on clay minerals. III. Nucleation and epitaxial growth of Zn phyllosilicate on the edges of hectorite. *Geochim. Cosmochim. Acta* **65**, 4155–4170.

Singh, B., Gilkes, R.J., 1996. Nature and properties of iron rich glaebules and mottles from some south-west Australian soils. *Geoderma* **71**, 95–120.

Smith, R.M., Martell, A.E., 1976. *Critical Stability Constants, vol. 4. Inorganic Complexes*. Plenum Press, New York and London.

Smith, R.M., Martell, A.E., 1989. *Critical Stability Constants, vol. 3. Other Organic Ligands*. Plenum Press, New York.

Soulier, A., Regeard, A., Trolard, F., 1994. Calibration of selective extraction technique by citrate–bicarbonate on the basis of experimental dissolution of synthetic iron oxides*Proc. 15th World Cong. Soil Sci.*, 3b-II. Mexican Society of Soil Science, Acapulco, Mexico, pp. 216–217.

Spadini, L., Manceau, A., Schindler, P.W., Charlet, L., 1994. Structure and stability of Cd^{2+} surface complexes on ferric oxides. *J. Colloid Interf. Sci.* **168**, 73–86.

Steele, M.C., Pichtel, J., 1998. Ex-situ remediation of a metal-contaminated Superfund soil using selective extractants. *J. Environ. Eng. ASCE* **124**, 639–645.

Straub, K.L., Schink, B., 2004. Ferrihydrite reduction by *Geobacter* species is stimulated by secondary bacteria. *Arch. Microbiol.* **182**, 175–181.

Strawn, D.G., Sparks, D.L., 2000. Effects of soil organic matter on the kinetics and mechanisms of Pb(II) sorption and desorption in soil. *Soil Sci. Soc. Am. J.* **64**, 144–156.

Strawn, D., Doner, H., Zavarin, M., McHugo, S., 2002. Microscale investigation into the geochemistry of arsenic, selenium and iron in soil developed in pyritic shale materials. *Geoderma* **108**, 237–257.

Sun, B., Zhao, F.J., Lombi, E., McGrath, S.P., 2001. Leaching of heavy metals from contaminated soils using EDTA. *Environ. Pollut.* **113**, 111–120.

Sutton, S.R., Rivers, M.L., Chien, S.H., 1999. Hard X-ray synchrotron microprobe techniques and applications. In: Schulze, D., Bertsch, P., Stucki, J. (Eds.), *Synchrotron X-ray Methods in Clay Science*. The Clay Minerals Society of America, pp. 146–163.

Sutton, S.R., Bertsch, P.M., Newville, M., Rivers, M., Lanzirotti, A., Eng, P., 2002. Microfluorescence and microtomography analyses of heterogeneous earth and environmental materials. In: Fenter, P.A., Rivers, M.L., Sturchio, N.C., Sutton, S.R. (Eds.), *Applications of Synchrotron Radiation in Low-Temperature Geochemistry and Environmental Science*, vol. 49. Mineralogical Society of America, pp. 429–478.

Tandy, S., Bossart, K., Mueller, R., Ritschel, J., Hauser, L., Schulin, R., Nowack, B., 2004. Extraction of heavy metals from soils using biodegradable chelating agents. *Environ. Sci. Technol.* **38**, 937–944.

Teo, B.K., 1986. *EXAFS: Basic Principles and Data Analysis*. Springer-Verlag, Berlin.

Tessier, A., Campbell, P.G.C., Bisson, M., 1979. Sequential extraction procedure for the speciation of particulate trace metals. *Anal. Chem.* **51**, 844–851.

Thayalakumaran, T., Robinson, B.H., Vogeler, I., Scotter, D.R., Clothier, B.E., Percival, H.J., 2003a. Plant uptake and leaching of copper during EDTA-enhanced phytoremediation of repacked and undisturbed soil. *Plant Soil* **254**, 415–423.

Thayalakumaran, T., Vogeler, I., Scotter, D.R., Percival, H.J., Robinson, B.H., Clothier, B.E., 2003b. Leaching of copper from contaminated soil following the application of EDTA. I. Repacked soil experiments and a model. *Aust. J. Soil Res.* **41**, 323–333.

Thayalakumaran, T., Vogeler, I., Scotter, D.R., Percival, H.J., Robinson, B.H., Clothier, B.E., 2003c. Leaching of copper from contaminated soil following the application of EDTA. II. Intact core experiments and model testing. *Aust. J. Soil Res.* **41**, 335–350.

Thiry, M., Van Oort, F., 1999. Les phases minerales majeures et mineures d'une friche industrielle de métallurgie des métaux non-ferreux: Etat d'altération, évolution géochimique et devenir des métaux polluants du site de Mortagne-du-Nord. In: *Spéciation des métaux dans le sol*. Ecrin Editions, Paris, pp. 108–135.

Thiry, M., Huet Taillanter, S., Schmitt, J.M., 2002. The industrial waste land of Mortagne-du-Nord (59)–I–Assesment, composition of the slags, hydrochemistry, hydrology and estimate of the outfluxes. *Bull. Soc. Geol. Fr.* **173**, 369–381.

Tichy, R., Rulkens, W.H., Grotenhuis, J.T.C., Nydl, V., Cuypers, C., Fajtl, J., 1998. Bioleaching of metals from soils or sediments. *Water Sci. Technol.* **37**, 119–127.

Trivedi, P., Dyer, J.A., Sparks, D.L., Pandya, K., 2004. Mechanistic and thermodynamic interpretations of zinc sorption onto ferrihydrite. *J. Colloid Interf. Sci.* **270**, 77–85.

Trolard, F., Bourrie, G., Jeanroy, E., Herbillon, A.J., Martin, H., 1995. Trace metals in natural iron oxides from laterites: A study using selective kinetic extraction. *Geochim. Cosmochim. Acta* **59**, 1285–1297.

Van Benschoten, J.E., Matsumoto, M.R., Young, W.H., 1997. Evaluation and analysis of soil washing for seven lead-contaminated soils. *J. Environ. Eng. ASCE* **123**, 217–224.

Vandevivere, P., Hammes, F., Verstraete, W., Feijtel, T., Schowanek, D., 2001a. Metal decontamination of soil, sediment, and sewage sludge by means of transition metal chelant [S,S]-EDDS. *J. Environ. Eng. ASCE* **127**, 802–811.

Vandevivere, P.C., Saveyn, H., Verstraete, W., Feijtel, T.C.J., Schowanek, D.R., 2001b. Biodegradation of metal–[S,S]-EDDS complexes. *Environ. Sci. Technol.* **35**, 1765–1770.

Vassil, A.D., Kapulnik, Y., Raskin, I., Salt, D.E., 1998. The role of EDTA in lead transport and accumulation by Indian mustard. *Plant Physiol.* **117**, 447–453.

Voegelin, A., Pfister, S., Scheinost, A.C., Marcus, M.A., Kretzschmar, R., 2005. Changes in zinc speciation in field soil after contamination with zinc oxide. *Environ. Sci. Technol.* **39**, 6616–6623.

Wasay, S.A., Barrington, S.F., Tokunaga, S., 1998. Remediation of soils polluted by heavy metals using salts of organic acids and chelating agents. *Environ. Technol.* **19**, 369–379.

Wasserman, S.R., 1997. The analysis of mixtures: Application of principal component analysis to XAS spectra. *J. Phys. IV* **7**, 203–205.

Wasserman, S.R., Allen, P.G., Shuh, D.K., Bucher, J.J., Edelstein, N.M., 1999. EXAFS and principal component analysis: a new shell game. *J. Synchrotron Rad.* **6**, 284–286.

Waychunas, G.A., Fuller, C.C., Davis, J.A., 2002. Surface complexation and precipitate geometry for aqueous Zn(II) sorption on ferrihydrite I: X-ray absorption extended fine structure spectroscopy analysis. *Geochim. Cosmochim. Acta* **67**, 2649–2662.

Whitburn, J.S., Wilkinson, S.D., Williams, D.R., 1999. Chemical speciation of ethylenediamine–*N*,*N*'-disuccinic acid (EDDS) and its metal complexes in solution. *Chem. Spec. Bioavailab.* **11**, 85–93.

Wolery, T., 1992. *EQ3/6. A Software Package for Geochemical Modelling of Aqueous Systems: Package Overview and Installation Guide (Version 7.0). Technical Report UCRL-MA-110662 PT*. Lawrence Livermore National Laboratory, USA.

Wu, J., Hsu, F.C., Cunningham, S.D., 1999. Chelate-assisted Pb phytoextraction: Pb availability, uptake, and translocation constraints. *Environ. Sci. Technol.* **33**, 1898–1904.